IEEE Access
Multidisciplinary | Rapid Review | Open Access Journal

SPECIAL SECTION ON ADVANCES IN STATISTICAL CHANNEL MODELING FOR FUTURE WIRELESS COMMUNICATIONS NETWORKS

Received June 28, 2019, accepted July 11, 2019, date of publication July 24, 2019, date of current version August 13, 2019.

Digital Object Identifier 10.1109/ACCESS.2019.2930931

Higher Order Statistics in a mmWave Propagation Environment

ANDRÉ ANTÔNIO DOS ANJOS[1], TIAGO REIS RUFINO MARINS[1], CARLOS RAFAEL NOGUEIRA DA SILVA[2], VICENT MIQUEL RODRIGO PEÑARROCHA[3], LORENZO RUBIO[3], (Senior Member, IEEE), JUAN REIG[3], (Senior Member, IEEE), RAUSLEY ADRIANO AMARAL DE SOUZA[1], (Member, IEEE), AND MICHEL DAOUD YACOUB[2], (Member, IEEE)

[1]National Institute of Telecommunications (INATEL), 37540-000 Santa Rita do Sapucaí, Brazil
[2]Wireless Technology Laboratory (WissTek), Department of Communications, School of Electrical and Computation Engineering, State University of Campinas, DECOM/FEEC/UNICAMP, 13083-852 Campinas, Brazil
[3]Telecommunications and Multimedia Applications Research Institute (iTEAM), Universitat Politècnica de València, 46022 Valencia, Spain

Corresponding author: Rausley Adriano Amaral de Souza (rausley@inatel.br)

This work was supported in part by the Conselho Nacional de Desenvolvimento Científico e Tecnológico (CNPq) under Grant 304248/2014-2 and Grant 308365/2017-8, in part by the Rede Nacional de Ensino e Pesquisa (RNP), with resources from Ministério da Ciência, Tecnologia, Inovações e Comunicações (MCTIC), through the Radiocommunication Reference Center [Centro de Referência em Radiocomunicações (CRR)] Project of the National Institute of Telecommunications [Instituto Nacional de Telecomunicações (INATEL)], Brazil, under Grant 01250.075413/2018-04, and in part by the Ministerio de Economía, Industria y Competitividad of the Spanish Government through the Agencia Estatal de Investigación (AEI) and the Fondo Europeo de Desarrollo Regional (FEDER) under Project TEC2017-86779-C2-2-R.

ABSTRACT A thorough measurement campaign in an indoor environment at the millimeter-wave band is carried out with an aim at characterizing the short-term fading channel in terms of its higher-order statistics. The measurements are conducted in a variety of scenarios, with frequencies ranging from 55 to 65 GHz, in line-of-sight and non-line-of-sight conditions, and combinations of horizontal and vertical polarizations at both the transmitter and the receiver. A number of fading models are tested, namely Rayleigh, Rice, Nakagami-m, α-μ, κ-μ, η-μ, and α-η-κ-μ. The main second-order statistics under analysis are the level crossing rate (LCR) and average fade duration (AFD) both given per distance unit. From the experimental data, the parameters of these statistics are estimated, and the corresponding curves of the theoretical models are compared with the empirical ones and the best model is selected. Additionally, the study of the very general distribution, namely α-η-κ-μ, is advanced, in which new expressions for time-/distance-domain LCR and AFD are derived using an envelope-based approach. Such an approach leads to integral-form formulations with much less computational complexity and computes rapidly compared with the already existing ones presented elsewhere, also given in the integral form. Furthermore, a series of expansion expression for the α-η-κ-μ time-/distance-domain LCR is then derived that improves even further the computational time.

INDEX TERMS Level crossing rate, measurement campaign, millimeter wave communication, small-scale fading, statistical analysis.

I. INTRODUCTION

Recent studies forsee a remarkable increase in the data transmission rate, aiming to meet the numerous applications that are emerging with the advent of the new generation of wireless communications, the 5th generation (5G). Some billions of connected Internet of things (IoT) devices are predicted worldwide by the year 2025 [1] with different sectors investing in high connectivity. The automotive industry, for instance, are committed to technologies for the development of cars that communicate with each other, also called vehicle-to-vehicle (V2V) communication [2]. In rural areas, the use of new technologies, such as device-to-device (D2D) communication, is also present, where the devices share information with a database to assist in the plantation process from sowing to harvesting [3]. All of these and other scenarios

The associate editor coordinating the review of this manuscript and approving it for publication was Daniel Benevides Da Costa.

of applications are to be addressed by future generations of wireless communications. To meet such a demand, it is estimated that the data rate offered by the 5G should be 100 to 1000 times greater than that of the current systems [4]. As a consequence, the increase in the bandwidth is imperious. The sub-6 GHz frequency bands are practically all occupied, and the small number of band gaps that still exist will not be enough to accommodate the required bandwidth for the 5G. Standard organizations, such as 3GPP, have already signaled that frequency bands above 10 GHz, the so-called millimeter-wave (mmWave) bands, should be used to cope with demands that require high transmission rates [5]. The high spectral availability renders the use of this band very advantageous in spite of the technical challenges to be faced. In mmWave band some phenomena are more or less strongly perceived as compared to lower frequency bands. For example, signal attenuation is higher and penetration into solid objects is problematic [6]. Also, rain may be a source of signal outage, because the rain drops are at the order of magnitude of the wavelength, operating as scatterers. At higher frequencies, the different propagation environments are more strongly perceived rendering multipath clustering a common phenomenon. In addition, medium nonlinearity is also more noticeable and may have a strong impact in the propagation of the signal. For these and other peculiarities, the propagation conditions at this band remain to be better understood.

A large number of different measurements campaigns has been conducted with the aim to model the propagation channel in mmWave frequencies [7]–[12]. Large-scale path loss models have been extensively explored [13]–[15]. Although extremely important and drastically affecting the performance of wireless communications systems, the statistics of small-scale fading at mmWave frequencies have thus far received little attention. Interestingly, many of the stochastic channel models available in literature assume Rayleigh or Rice distributions for the small-scale fading amplitudes in non-line-of-sight (nLoS) and line-of-sight (LoS) scenarios, respectively [10], [11], [16]–[18]. In [16], the short-term fading amplitude for LoS measurements taken in three corridors of an office block at frequency 60 GHz with a bandwidth of 1 GHz has been modeled as a Rician distribution. Values of mean and standard deviation of the Rice factor have been reported for two antenna types, i.e. an open-ended waveguide and lens. Other interesting results have been shown in [17], where the small-scale fading statistics obtained from a 28 GHz outdoor measurement campaign revealed that the Rician model was more suitable than Rayleigh even in nLoS conditions. A glance at some of the published works for different mmWave scenarios e.g. [17]–[19], shows that more elaborate fading models must be exercised so that the true behavior of the fading channel can be better captured.

In most cases, the analysis focuses on well established statistical distributions, including Nakagami-*m*, Rice, Rayleigh, and Weibull, which are certainly applicable to describe the small-scale fading in several multipath propagation situations. However, the diversity of scenarios imagined for the mmWave band will certainly lead to a variety of propagation conditions, which are less likely to be accommodated by the classical fading models. In these cases, more flexible statistical models, such as α-μ [20], κ-μ [21], η-μ [21], α-κ-μ [22], and α-η-μ [22] may be useful. Some research has already assessed the use of multiparameter distributions to model field data in mmWave frequencies [19], [23], [24]. However, the results obtained in one or another case have not reproduced some peculiar effect of the behavior of the signal in mmWave band [19], being desirable the use of more flexible models.

A very general statistical model has been proposed in [25] namely α-η-κ-μ. It is constructed with parameters that take into account the main physical phenomena affecting the signal propagation, including nonlinearity of the medium, multipath clustering, power of the dominant components, and power of the scattered waves. Due to its multiparameter characteristic, this model is capable to accommodate an enormous number of fading scenarios. It comprises all of the most relevant complex-based fading scenarios found in the literature. It is indeed more mathematically involving, but its flexibility renders it highly adjustable to more complex fading scenarios. Very recently, in [6] higher order statistics for the α-η-κ-μ model have been derived, namely time-domain level crossing rate ($\mathrm{LCR_t}$), time-domain average fade duration ($\mathrm{AFD_t}$), and time-domain phase crossing rate ($\mathrm{PCR_t}$).[1] The authors also demonstrate an interesting behavior of α-η-κ-μ model exploring regions with non-unimodality effects of measurement data probability density function (PDF).

In this paper, an exhaustive mmWave measurement campaign is carried out in an indoor environment aiming at characterizing the higher-order short-term fading channel behavior. The chosen frequencies cover the full range from 55 GHz to 65 GHz band, in LoS and nLoS conditions, with combinations of horizontal and vertical polarizations at both transmitter and receiver. Different fading scenarios are tested, namely Rayleigh, Rice, Nakagami-*m*, α-μ, κ-μ, η-μ, and α-η-κ-μ. From the experimental data, the parameters of these statistics are estimated and the corresponding curves of the theoretical models are compared with the empirical ones and the best model is selected. In addition to these in-depth practical measurements, analytical expressions in terms of a single proper integral for $\mathrm{LCR_t}$ and $\mathrm{AFD_t}$ and analytical expressions for $\mathrm{LCR_t}$ in terms of a series expansion for the α-η-κ-μ fading model are derived.

This paper is organized as follows. Section II briefly revisits the α-η-κ-μ fading model. Section III derives the higher order statistics of the α-η-κ-μ using the envelope-based approach. Section IV presents the $\mathrm{LCR_t}$ in terms of a series expansion. Section V shows theoretical expressions of LCR in space-domain for all distributions tested in the experimental part of the work. The setup environment and measurement

[1] The acronyms for LCR, AFD, and phase crossing rate (PCR) are followed by a subscript t to denote that these statistics are obtained having as attribute the time (level crossing per time, time below level, and phase crossing per time).

procedure along with the goodness-of-fit criteria used are described in Section VI. Section VII compares empirical and theoretical higher-order statistics and indicates the model with the best fitting performance. Section VIII draws some conclusions.

II. THE α-η-κ-μ FADING MODEL REVISITED

The complex-based α-η-κ-μ fading model proposed in [25] considers independent in-phase and quadrature components of the fading signals with different attributes, resulting in the complex signal $S = R^{\frac{\alpha}{2}} \exp(j\Theta) = X + jY$. The densities of the in-phase component X and quadrature component Y were derived from a general random variable Z defined in [21] as

$$Z^2 = \sum_{i=1}^{\mu_z} (Z_i + \lambda_i)^2 , \tag{1}$$

in which, (i) Z may denote either X or Y; (ii) Z_i are independent zero-mean-σ_z^2-variance Gaussian processes; (iii) λ_i^2 is the power of a dominant component in each cluster; and μ_z denotes the number of multipath clusters. The corresponding PDF $f_Z(z)$ is found in [26, Eqn. (15)]. In this approach, it is possible to obtain the statistical information about both envelope and phase. On the other hand, in the analysis for which the phase knowledge is not relevant, another approach can be used to obtain more simplified expressions, considering only envelope R of the signal, as detailed in [25, Sec. IV]. The α-η-κ-μ envelope R can be written as [25, Eqn. (9)]

$$R^\alpha = \sum_{i=1}^{\mu_x} (X_i + \lambda_{x_i})^2 + \sum_{i=1}^{\mu_y} (Y_i + \lambda_{y_i})^2, \tag{2}$$

in which: $\alpha > 0$ quantifies the nonlinearity of the medium; X_i and Y_i are mutually zero-mean independent Gaussian processes with variances σ_x^2 and σ_y^2, respectively; λ_{x_i} and λ_{y_i} are, respectively, the mean values of the in-phase and quadrature components of the multipath waves of ith cluster; and μ_x and μ_y are the number of multipath clusters of in-phase and quadrature components, respectively. The multiparameter PDF of the α-η-κ-μ envelope model is presented in three parametrization formats, namely Raw [25, Eqn. (17)], Local [25, Eqn. (23)], and Global Parametrization [25, Eqn. (29)]. In the Global Parametrization, the following are the parameters (all positive): (i) α denotes the nonlinearity of the medium; (ii) $\eta = \mu_x\sigma_x^2/(\mu_y\sigma_y^2)$ defines the ratio of the total power of the in-phase and quadrature scattered waves of the multipath clusters; (iii) $\kappa = (\lambda_x^2 + \lambda_y^2)/(\mu_x\sigma_x^2 + \mu_y\sigma_y^2)$ gives the ratio of the total power of the dominant components and the total power of scattered waves; (iv) $\mu = (\mu_x + \mu_y)/2$ concerns the number of multipath clusters; (v) $p = \mu_x/\mu_y$ depicts the ratio of the number of multipath clusters of in-phase and quadrature signals; (vi) $q = \lambda_x^2\mu_y\sigma_y^2/(\lambda_y^2\mu_x\sigma_x^2)$ describes the ratio of two ratios: the ratio of the power of the dominant components to the power of the scattered waves of the in-phase signal and its counterpart for the quadrature signal; and (vii) $\hat{r}^\alpha = \mathbb{E}(R^\alpha) = \mu_x\sigma_x^2 + \lambda_x^2 + \mu_y\sigma_y^2 + \lambda_y^2$, with $\mathbb{E}(\cdot)$ standing for the expectation operator. The number of distributions obtainable from the α-η-κ-μ model as particular cases is enormous and is far from having been explored in its entirety yet. A detailed explanation for the known special cases and also the meaning of each parameter can be found in [25]. A great number of well-known distributions, and others not yet available in the literature, can be obtained as the particular cases of the α-η-κ-μ fading model. Among them, the three-fading-parameter distributions (α-κ-μ and α-η-μ), the two-fading-parameter distributions (α-μ, η-μ, κ-μ and Beckmann (η-κ)), the one-fading-parameter ones, namely, Nakagami-m, Weibull, Hoyt, and Rice, and no-fading-parameter ones, namely, Rayleigh, semi-Gaussian, and negative exponential. A detailed explanation for the special cases can be found in [25, Section VI].

In addition to the aforementioned parameters employed in the first-order statistics of the general α-η-κ-μ fading model, it is necessary to define some others to be used in its higher-order statistics. We define the following: (i) $\ddot{\psi}(0)$, as the mean of the second derivative with respect to time of the time autocorrelation function at zero; (ii) d, as the imbalance of the second derivative with respect to time of the time autocorrelation function at zero between in-phase and quadrature components. Consequently, (i) $2(-\ddot{\psi}(0))^{1/2} = (-\ddot{\psi}_x(0))^{1/2} + (-\ddot{\psi}_y(0))^{1/2}$; (ii) $d = (-\ddot{\psi}_x(0))^{1/2}/(-\ddot{\psi}_y(0))^{1/2}$; (iii) $(-\ddot{\psi}_x(0))^{1/2} = 2d(-\ddot{\psi}(0))^{1/2}/(1+d)$; (iv) $(-\ddot{\psi}_y(0))^{1/2} = 2(-\ddot{\psi}(0))^{1/2}/(1+d)$.

III. HIGHER ORDER STATISTICS USING THE ENVELOPE-BASED APPROACH

The α-η-κ-μ higher order statistics addressed in this section concern those related to the time derivative of the envelope of the signal. We start by rewriting (2) as

$$R^\alpha = U^2 + V^2, \tag{3}$$

where the PDFs $f_U(u)$ and $f_V(v)$ of U and V follow two κ-μ envelope PDFs with respective parameters ($\kappa_x = \lambda_x^2/(\mu_x\sigma_x^2)$, $\mu_x/2$) and ($\kappa_y = \lambda_y^2/(\mu_y\sigma_y^2)$, $\mu_y/2$). We then proceed by calculating the joint distribution of U, V and $\dot{R}$, in which the dot symbol signifies the time derivative of the variate. Then, we proceed by making a transformation of variables to obtain the joint distribution of R, $\dot{R}$ and V. The aim is to obtain some joint distributions of combinations of R, $\dot{R}$ and V with a view at deriving some important metrics, namely LCR and AFD.

A. PDF OF $\dot{Z}$

From Section II, the in-phase and quadrature components of the α-η-κ-μ signal follow the distribution as given in [26, Eqn. (15)] with the corresponding physical model given by (1). As clearly stated in [25], the power of the quadrature process of the α-η-κ-μ model is that of a κ-μ power with parameters $\kappa_z = \lambda_z^2/(\mu_z\sigma_z^2)$ and $\mu_z/2$. Hence, the said quadrature process takes the form of that of a κ-μ one with the respective parameters. In [27], such a process has been thoroughly investigated. Now, resorting on the findings of [27], we maintain that Z and $\dot{Z}$ are independent processes

with the PDF $f_{\dot{Z}}(\dot{z})$ of $\dot{Z}$ being that of a zero-mean Gaussian, whose variance is defined as $\sigma_{\dot{z}}^2$. Thus

$$f_{\dot{Z}}(\dot{z}) = \frac{1}{\sqrt{-2\pi\sigma_z^2\ddot{\psi}_z(0)}} \exp\left(\frac{\dot{z}}{2\sigma_z^2\ddot{\psi}_z(0)}\right), \tag{4}$$

in which $\psi_z(\tau)$ is the correlation as a function of time τ, and $\ddot{\psi}_z(0)$ is its time derivative at $\tau = 0$.

B. JOINT PDF OF U, V, $\dot{R}$

We start by taking the time derivative on both sides of (3) and isolating $\dot{R}$, yielding

$$\dot{R} = \frac{2U\dot{U} + 2V\dot{V}}{\alpha R^{\alpha-1}}. \tag{5}$$

Comparing (1), (2) and (3), it is straightforward to conclude that the PDFs $f_{\dot{U}}(\dot{u})$ and $f_{\dot{V}}(\dot{v})$ of $\dot{U}$ and $\dot{V}$ follow that of $\dot{Z}$ with the respective parameters $\sigma_{\dot{u}}^2 = 2\pi^2 f_x^2\sigma_x^2$ and $\sigma_{\dot{v}}^2 = 2\pi^2 f_y^2\sigma_y^2$. Therefore, the PDF $f_{\dot{R}|U,V}(\dot{r}|u,v)$ is that of the sum two Gaussian random process, leading to

$$f_{\dot{R}|U,V}(\dot{r}|u,v) = \frac{1}{\sqrt{2\pi\sigma_{\dot{r}}^2}} \exp\left(-\frac{\dot{r}^2}{2\sigma_{\dot{r}}^2}\right), \tag{6}$$

where $\dot{\sigma}_r = 2(u^2\dot{\sigma}_u^2 + v^2\dot{\sigma}_v^2)^{1/2}/(\alpha r^{\alpha-1})$. Consequently, $f_{U,V,\dot{R}}(u,v,\dot{r}) = f_{\dot{R}|U,V}(\dot{r}|u,v) \times f_U(u) \times f_V(v)$. Thus, the final joint PDF can be expressed as in (7), as shown at the bottom of this page, with $I_\upsilon(\cdot)$ representing the modified Bessel function of the first kind and order υ [28, Eqn. (8.406.5)].

C. JOINT PDF OF R, $\dot{R}$, V

The joint PDF $f_{R,\dot{R},V}(r,\dot{r},v)$ is obtained through variable transformations. Thus, $f_{R,\dot{R},V}(r,\dot{r},v) = |J| f_{U,V,\dot{R}}(u,v,\dot{r})$, where J is the Jacobian of the transformation, R is the signal envelope, $\dot{R}$ its time derivate and $U = \sqrt{R^\alpha - V^2}$, achieved manipulating (3). Now, carrying out the necessary algebraic manipulations and using $|J| = \alpha r^{\alpha-1}/(2\sqrt{|r^\alpha - v^2|})$, the joint PDF is presented in (8), as shown at the bottom of this page.

D. THE MARGINAL PDF OF $\dot{R}$

The marginal PDF of $\dot{R}$ can be derived by appropriate integrations of (7) or (8). Unfortunately, the integration of both equations with respect to U, V or R seems not to lead to closed forms and then the required marginal PDF are left in its integral forms as follows

$$f_{\dot{R}}(\dot{r}) = \int_0^\infty \int_0^\infty f_{U,V,\dot{R}}(u,v,\dot{r})\, du dv, \tag{9}$$

or

$$f_{\dot{R}}(\dot{r}) = \int_0^\infty \int_0^\infty f_{R,\dot{R},V}(r,\dot{r},v)\, du dv. \tag{10}$$

$$f_{U,V,\dot{R}}(u,v,\dot{r}) = \frac{\alpha\mu_x\mu_y \left(\frac{\lambda_x^2}{\mu_x\sigma_x^2}\right)^{\frac{1}{2}\left(1-\frac{\mu_x}{2}\right)} \left(\frac{u}{\sqrt{\lambda_x^2+\mu_x\sigma_x^2}}\right)^{\frac{\mu_x}{2}} \left(\frac{\lambda_y^2}{\mu_y\sigma_y^2}\right)^{\frac{1}{2}\left(1-\frac{\mu_y}{2}\right)} \left(\frac{v}{\sqrt{\lambda_y^2+\mu_y\sigma_y^2}}\right)^{\frac{\mu_y}{2}}}{2\pi\sqrt{-2\pi^{-1}\left(\lambda_x^2+\mu_x\sigma_x^2\right)\left(\lambda_y^2+\mu_y\sigma_y^2\right)\left(u^2+v^2\right)^{\frac{2-2\alpha}{\alpha}}\left(\ddot{\psi}_x(0)u^2\sigma_x^2+\ddot{\psi}_y(0)v^2\sigma_y^2\right)}}$$
$$\times \exp\left(-\left(\frac{\lambda_x^2}{2\sigma_x^2}+\frac{\lambda_y^2}{2\sigma_y^2}\right) - \left(\frac{u^2\mu_x\left(1+\frac{\lambda_x^2}{\mu_x\sigma_x^2}\right)}{2\left(\lambda_x^2+\mu_x\sigma_x^2\right)} + \frac{v^2\mu_y\left(1+\frac{\lambda_y^2}{\mu_y\sigma_y^2}\right)}{2\left(\lambda_y^2+\mu_y\sigma_y^2\right)}\right) + \frac{\left(u^2+v^2\right)^{\frac{-2+2\alpha}{\alpha}}\dot{r}^2\alpha^2}{8\left(\ddot{\psi}_x(0)u^2\sigma_x^2+\ddot{\psi}_y(0)v^2\sigma_y^2\right)}\right)$$
$$\times \left(1+\frac{\lambda_x^2}{\mu_x\sigma_x^2}\right)^{\frac{1}{2}\left(1+\frac{\mu_x}{2}\right)} \left(1+\frac{\lambda_y^2}{\mu_y\sigma_y^2}\right)^{\frac{1}{2}\left(1+\frac{\mu_y}{2}\right)} I_{\frac{\mu_x}{2}-1}\left(\frac{u\lambda_x}{\sigma_x^2}\right) I_{\frac{\mu_y}{2}-1}\left(\frac{v\lambda_y}{\sigma_y^2}\right) \tag{7}$$

$$f_{R,\dot{R},V}(r,\dot{r},v) = \frac{\alpha^2 r^{\alpha-1}\,\mu_x\mu_y \left(1+\frac{\lambda_x^2}{\mu_x\sigma_x^2}\right)^{\left(\frac{1}{2}+\frac{\mu_x}{4}\right)} \left(1+\frac{\lambda_y^2}{\mu_y\sigma_y^2}\right)^{\left(\frac{1}{2}+\frac{\mu_y}{4}\right)} \left(\frac{\lambda_x^2}{\mu_x\sigma_x^2}\right)^{\left(\frac{1}{2}-\frac{\mu_x}{4}\right)} \left(\frac{\lambda_y^2}{\mu_y\sigma_y^2}\right)^{\left(\frac{1}{2}-\frac{\mu_y}{4}\right)}}{4\pi\sqrt{-2\pi^{-1}r^{2-2\alpha}\left(r^\alpha-v^2\right)\left(\lambda_x^2+\mu_x\sigma_x^2\right)\left(\lambda_y^2+\mu_y\sigma_y^2\right)\left(\left(r^\alpha-y^2\right)\ddot{\psi}_x(0)\sigma_x^2+\ddot{\psi}_y(0)v^2\sigma_y^2\right)}}$$
$$\times \exp\left(-\frac{\lambda_x^2}{2\sigma_x^2}-\frac{\lambda_y^2}{2\sigma_y^2}-\frac{\left(r^\alpha-v^2\right)\left(\mu_x+\frac{\lambda_x^2}{\sigma_x^2}\right)}{2\left(\lambda_x^2+\mu_x\sigma_x^2\right)}-\frac{v^2\left(\mu_y+\frac{\lambda_y^2}{\sigma_y^2}\right)}{2\left(\lambda_y^2+\mu_y\sigma_y^2\right)}+\frac{\alpha^2 r^{2\alpha-2}\dot{r}^2}{8\left(\ddot{\psi}_x(0)\left(r^\alpha-v^2\right)\sigma_x^2+\ddot{\psi}_y(0)v^2\sigma_y^2\right)}\right)$$
$$\times \left(\sqrt{\frac{r^\alpha-v^2}{\lambda_x^2+\mu_x\sigma_x^2}}\right)^{\frac{\mu_x}{2}} \left(\frac{v}{\sqrt{\lambda_y^2+\mu_y\sigma_y^2}}\right)^{\frac{\mu_y}{2}} I_{\frac{\mu_x}{2}-1}\left(\frac{\sqrt{r^\alpha-v^2}\lambda_x}{\sigma_x^2}\right) I_{\frac{\mu_y}{2}-1}\left(\frac{v\lambda_y}{\sigma_y^2}\right) \tag{8}$$

E. LEVEL CROSSING RATE

The $\mathrm{LCR_t}$ is a second order statistic that yields the average number of upward (or downward) crossings per second at a given level R. By definition, the $\mathrm{LCR_t}$ of a continuous process can be calculated as

$$N_R(r) = \int_0^\infty \dot{r} f_{R,\dot{R}}(r,\dot{r})\, d\dot{r}. \tag{11}$$

The calculation of the α-η-κ-μ $\mathrm{LCR_t}$ involves a cumbersome task because there is no closed-form expression of $f_{R,\dot{R}}(r,\dot{r})$. This joint PDF can be expressed as

$$f_{R,\dot{R}}(r,\dot{r}) = \int_0^{\sqrt{r^\alpha}} f_{R,\dot{R},V}(r,\dot{r},v)\, dv. \tag{12}$$

Substituting (12) into (11) and changing the order of integration it is possible to write the $\mathrm{LCR_t}$ as

$$N_R(r) = \int_0^{\sqrt{r^\alpha}} \int_0^\infty \dot{r} f_{R,\dot{R},V}(r,\dot{r},v)\, d\dot{r} dv. \tag{13}$$

Let the innermost integral be denoted as the function $N_R(r,v)$. Thus

$$N_R(r,v) = \int_0^\infty \dot{r} f_{R,\dot{R},V}(r,\dot{r},v)\, d\dot{r}. \tag{14}$$

Its important to note that $N_R(r,v)$ is not the $\mathrm{LCR_t}$ but an intermediate function created to render the calculation possible. Fortunately, it is possible to solve the integral in $\dot{r}$. Hence, $N_R(r,v)$ is found in a exact manner as (15), as shown at the bottom of this page. The function $N_R(r,v)$ can also be rewritten in terms of the Global parametrization as given in (16), as shown at the bottom of this page.

Note that the $\mathrm{LCR_t}$ can now be solved by numerically evaluating a single integral, as follows

$$N_R(r) = \int_0^{\sqrt{r^\alpha}} N_R(r,v) dv. \tag{17}$$

It is important to emphasize that (17) is equivalent to that found in [6, Eqn. (11)], however, its mathematical complexity has been drastically diminished, hence improving the computational costs involving the $\mathrm{LCR_t}$ calculation.

F. AVERAGE FADE DURATION

The $\mathrm{AFD_t}$ of a fading signal envelope, $T_R(r)$, is defined as the average time that the signal spends below the threshold level R. It is related to the $\mathrm{LCR_t}$ through the relationship

$$T_R(r) = \frac{F_R(r)}{N_R(r)}, \tag{18}$$

where $F_R(r)$ is the cumulative distribution function (CDF) of the random variable R. The CDF can be calculated in a exact

$$\begin{aligned} N_R(r,v) = {} & \frac{\alpha^2 r^{-1+\alpha} \mu_x \mu_y \left(\frac{\lambda_x^2}{\mu_x\sigma_x^2}\right)^{\left(\frac{1}{2}-\frac{\mu_x}{4}\right)} \left(\frac{\lambda_y^2}{\mu_y\sigma_y^2}\right)^{\left(\frac{1}{2}-\frac{\mu_y}{4}\right)} \left(1+\frac{\lambda_x^2}{\mu_x\sigma_x^2}\right)^{\left(\frac{1}{2}+\frac{\mu_x}{4}\right)} \left(1+\frac{\lambda_y^2}{\mu_y\sigma_y^2}\right)^{\left(\frac{1}{2}+\frac{\mu_y}{4}\right)}}{4\pi\sqrt{-2r^{2-2\alpha}\left(r^\alpha-y^2\right)\left(\lambda_x^2+\mu_x\sigma_x^2\right)\left(\lambda_y^2+\mu_y\sigma_y^2\right)\left(\ddot{\psi}_x(0)\left(r^\alpha-v^2\right)\sigma_x^2+\ddot{\psi}_y(0)v^2\sigma_y^2\right)}} \\ & \times \exp\left(-\frac{\lambda_x^2}{2\sigma_x^2}-\frac{r^\alpha-v^2}{2\sigma_x^2}-\frac{\lambda_y^2}{2\sigma_y^2}+\frac{r^{-2+2\alpha}\dot{r}^2\alpha^2}{8\left(\ddot{\psi}_x(0)\left(r^\alpha-v^2\right)\sigma_x^2+\ddot{\psi}_y(0)v^2\sigma_y^2\right)}-\frac{y^2}{2\sigma_y^2}\right) \\ & \times \left(\sqrt{\frac{r^\alpha-v^2}{\lambda_x^2+\mu_x\sigma_x^2}}\right)^{\frac{\mu_x}{2}} \left(\frac{v}{\sqrt{\lambda_y^2+\mu_y\sigma_y^2}}\right)^{\frac{\mu_y}{2}} I_{\frac{\mu_x}{2}-1}\left(\frac{\sqrt{r^\alpha-v^2}\lambda_x}{\sigma_x^2}\right) I_{\frac{\mu_y}{2}-1}\left(\frac{v\lambda_y}{\sigma_y^2}\right) \end{aligned} \tag{15}$$

$$\begin{aligned} N_R(r,v) = {} & \frac{4\mu(pv^2+d^2(r^\alpha-v^2)\eta)(1+q\eta)\sqrt{-\ddot{\psi}(0)(1+\eta)(1+\kappa)\mu p\pi^{-1}}}{(1+d)(1+p)\sqrt{(r^\alpha-v^2)(1+\kappa+\eta(q+\kappa))\eta(1+q(\eta+\kappa+\eta\kappa))(1+p)\hat{r}^\alpha(pv^2+d^2(r^\alpha-v^2)\eta)}} \\ & \times \left(\frac{(1+\eta)\kappa}{1+q\eta}\right)^{\frac{1}{2}\left(1-\frac{\mu}{1+p}\right)} \left(\frac{q(1+\eta)\kappa}{1+q\eta}\right)^{\frac{1}{2}\left(1-\frac{p\mu}{1+p}\right)} \left(1+\frac{(1+\eta)\kappa}{1+q\eta}\right)^{\frac{1}{2}\left(1+\frac{\mu}{1+p}\right)} \left(1+\frac{q(1+\eta)\kappa}{1+q\eta}\right)^{\frac{1}{2}\left(1+\frac{p\mu}{1+p}\right)} \\ & \times \left(v\sqrt{\frac{(1+\eta)(1+q\eta)(1+\kappa)}{\hat{r}^\alpha(1+\kappa+\eta(q+\kappa))}}\right)^{\frac{\mu}{1+p}} \left(\sqrt{\frac{\left(r^\alpha-v^2\right)(1+\eta)(1+q\eta)(1+\kappa)}{\hat{r}^\alpha\eta(1+q(\eta+\kappa+\eta\kappa))}}\right)^{\frac{p\mu}{1+p}} \\ & \times \exp\left(-\frac{\mu\hat{r}^{-\alpha}(1+\eta)\left((1+pq)\hat{r}^\alpha\eta\kappa+(1+q\eta)\left(p\left(r^\alpha-v^2\right)+v^2\eta\right)(1+\kappa)\right)}{\eta(1+p)(1+q\eta)}\right) \\ & \times I_{\frac{\mu}{1+p}-1}\left(\frac{2\mu v(1+\eta)}{(1+p)}\sqrt{\frac{\kappa(1+\kappa)}{\hat{r}^\alpha(1+q\eta)}}\right) I_{\frac{p\mu}{1+p}-1}\left(\frac{2\mu p(1+\eta)}{(1+p)}\sqrt{\frac{q\kappa\left(r^\alpha-v^2\right)(1+\kappa)}{\hat{r}^\alpha\eta(1+q\eta)}}\right) \end{aligned} \tag{16}$$

$$N_R(r) = \frac{2d\sqrt{-\ddot{\psi}(0)}(\xi\mu)^{\mu-\frac{1}{2}}}{\sqrt{\pi}(1+d)\exp\left(\frac{(1+pq)\kappa\mu}{\delta}\right)}\left(\frac{\eta}{p}\right)^{\frac{1}{2}-\frac{p\mu}{1+p}}\frac{r^{\alpha\left(\mu-\frac{1}{2}\right)}}{\hat{r}^{\alpha\left(\mu-\frac{1}{2}\right)}}\exp\left(-\frac{\xi\mu p r^{\alpha}}{\eta\hat{r}^{\alpha}}\right)\sum_{n=0}^{\infty}\sum_{j=0}^{\infty}\frac{1}{j!}\left(\frac{p^2q\kappa\xi\mu^2r^{\alpha}}{\eta\delta\hat{r}^{\alpha}}\right)^{j}$$
$$\times\left(\frac{(p-\eta)\xi\mu r^{\alpha}}{\eta\hat{r}^{\alpha}}\right)^{n}L_n^{\frac{\mu}{1+p}-1}\left(-\frac{\eta\kappa\mu}{(p-\eta)\delta}\right){}_2\tilde{F}_1\left(-\frac{1}{2},n+\frac{\mu}{1+p};j+n+\mu;1-\frac{p}{d^2\eta}\right) \quad (21)$$

manner using the following triple integral

$$F_R(r) = \int_0^r\int_{-\infty}^{+\infty}\int_0^{\sqrt{r^{\alpha}}} f_{R,\dot{R},V}(r',\dot{r},v)dvd\dot{r}dr'. \quad (19)$$

Or, alternatively and preferably, it is possible to make use the CDF in an infinite series form, as presented in [25, Eqn. (26)], i.e.

$$F_R(r) = \frac{r^{\alpha\frac{\mu_x+\mu_y}{2}}\sum_{k=0}^{\infty}\frac{k!m_kL_k^{\frac{\mu_x+\mu_y}{2}}\left(\left(\frac{2}{\mu_x+\mu_y}+1\right)2r^{\alpha}\right)}{\left(\frac{\mu_x+\mu_y}{2}+1\right)_k}}{2^{\frac{\mu_x+\mu_y}{2}+1}\Gamma\left(\frac{\mu_x+\mu_y}{2}+1\right)\exp\left(\frac{r^{\alpha}}{2}\right)}, \quad (20)$$

where m_k for $k \geq 1$ is given by [25, Eqn. (16)], m_0 is given by [25, Eqn. (21)], $\Gamma(\cdot)$ is the Gamma function [29, Eqn. (6.1.1)] , $(a)_n$ is the Pochhammer symbol [29, Eqn. (6.1.22)], and $L_r^p(x) = r!L_r^{p-1}(x)$ is the generalized Laguerre polynomial [28, Eqn. (8.970/1)] with $L_r^{p-1}(x) = \sum_{j=0}^{r}(-1)^j\Gamma(p+r)x^j/(j!(r-j)!\Gamma(p+j))$.

Thus, the AFD_t may be solved by numerically evaluating (18) using (20) and (17).

IV. TIME-DOMAIN LEVEL CROSSING RATE - NOVEL SERIES REPRESENTATION

The LCR_t can be evaluated through (17). However, integral-form formulations can be computationally restrictive if performed repeatedly. An interesting and computationally efficient series representation is provided here as an alternative to compute the LCR_t. This is given in (21), as shown at the top of this page, for the Global parametrization with $\xi = (1+\eta)(1+\kappa)/(1+p)$ and $\delta = (1+q\eta)(1+p)/(1+\eta)$. In (21), ${}_2\tilde{F}_1(a,b;c;x) = {}_2F_1(a,b;c;x)/\Gamma(c)$ is the regularized form of the Gauss' hypergeometric function [29, Eqn. (15.1.1)]. Please refer to Appendix for the concerned proof.

It is important to remark that for $p = \eta$, an indeterminacy arises. However, this actually does not pose any problem since, as will be shown shortly, a simplification arises in this situation reducing the expression to a single series. In the next subsection, some particular cases will be derived which greatly simplifies this series.

A. LEVEL CROSSING RATE - SOME PARTICULAR CASES

1) PARTICULAR CASE: $q \to 0$

When q tends to zero, it is possible to ignore all terms in the summation of (21) over the index j, except for the index $j = 0$. After some algebraic manipulations, the LCR_t is given as

$$N_R(r) = \frac{2d\sqrt{-\ddot{\psi}(0)}(\xi\mu)^{\mu-\frac{1}{2}}}{\sqrt{\pi}(1+d)\exp\left(\frac{(1+\eta)\kappa\mu}{1+p}\right)}\left(\frac{\eta}{p}\right)^{\frac{1}{2}-\frac{p\mu}{1+p}}e^{-\frac{\xi\mu p r^{\alpha}}{\eta\hat{r}^{\alpha}}}$$
$$\times\frac{r^{\alpha\left(\mu-\frac{1}{2}\right)}}{\hat{r}^{\alpha\left(\mu-\frac{1}{2}\right)}}\sum_{n=0}^{\infty}\left(\frac{r^{\alpha}(p-\eta)\xi\mu}{\eta\hat{r}^{\alpha}}\right)^{n}L_n^{\frac{\mu}{1+p}-1}$$
$$\times\left(\frac{\eta(1+\eta)\kappa\mu}{(1+p)(\eta-p)}\right){}_2\tilde{F}_1\left(-\frac{1}{2},n+\frac{\mu}{1+p};n+\mu;1-\frac{p}{d^2\eta}\right). \quad (22)$$

2) PARTICULAR CASE: $p = \eta$

When $p = \eta$, an indeterminacy appears in (21). Such an issue can be resolved using the limit

$$\lim_{x\to 0}(xz)^nL_n^{\lambda-1}\left(-\frac{t}{x}\right) = \frac{(tz)^n}{\Gamma(1+n)}. \quad (23)$$

After the adequate algebraic manipulations in (21), the LCR_t is obtained as

$$N_R(r) = \frac{2d\sqrt{-\ddot{\psi}(0)}((1+\kappa)\mu)^{\mu-\frac{1}{2}}}{\sqrt{\pi}(1+d)\exp(\kappa\mu)}\frac{r^{\alpha\left(\mu-\frac{1}{2}\right)}}{\hat{r}^{\alpha\left(\mu-\frac{1}{2}\right)}}e^{-\frac{r^{\alpha}(1+\kappa)\mu}{\hat{r}^{\alpha}}}$$
$$\times\sum_{n=0}^{\infty}\sum_{j=0}^{\infty}\frac{1}{j!n!}\left(\frac{\kappa\mu^2(1+\kappa)\left(\frac{r}{\hat{r}}\right)^{\alpha}}{1+q\eta}\right)^{n}$$
$$\times\left(\frac{qr^{\alpha}\eta\kappa(1+\kappa)\mu^2}{(1+q\eta)\hat{r}^{\alpha}}\right)^{j}{}_2\tilde{F}_1\left(-\frac{1}{2},n+\frac{\mu}{1+\eta};\right.$$
$$\left.j+n+\mu;1-\frac{1}{d^2}\right). \quad (24)$$

It is possible to reduce the expression above to a single series by writing the hypergeometric function as a power series, performing the summation over the index j and finally over the infinite triangle $k = i - n$. After some tedious algebraic manipulations, the LCR_t is given in (25), as shown at the top of the next page, wherein ${}_2F_1(a,b;c;x)$ is a particular case of the generalized hypergeometric function [30, Eqn. (2.12.4.3)]. The series in (25) converges only when $d > 1/\sqrt{2}$. This presents no issue due to the inherent symmetry of the α-η-κ-μ fading model such that, outside the convergence region, the LCR_t can be evaluated using the symmetry $\{\alpha,\eta,\kappa,\mu,p,q,\ddot{\psi}(0),d\} = \{\alpha,1/\eta,\kappa,\mu,1/p,1/q,\ddot{\psi}(0),1/d\}$. It is worthy remarking that, while the PDF of the α-η-κ-μ reduces to that of the α-κ-μ such that parameters η and q vanishes, in the LCR_t

$$N_R(r) = \frac{2d\sqrt{-\ddot{\psi}(0)}((1+\kappa)\mu)^{\mu/2}}{\sqrt{\pi}(1+d)\exp(\kappa\mu)}\left(\frac{q\eta\kappa\mu}{1+q\eta}\right)^{\frac{1-\mu}{2}}\left(\frac{r}{\hat{r}}\right)^{\frac{\alpha\mu}{2}}\exp\left(-\frac{\mu(1+\kappa)r^\alpha}{\hat{r}^\alpha}\right)\sum_{k=0}^{\infty}\frac{\left(-\frac{1}{2}\right)_k\left(\frac{\mu}{1+\eta}\right)_k}{k!}\left(1-\frac{1}{d^2}\right)^k$$
$$\times\left(\frac{\sqrt{(1+q\eta)\hat{r}^\alpha}}{\sqrt{\eta q\kappa(1+\kappa)r^\alpha}\mu}\right)^k I_{k+\mu-1}\left(\frac{2r^{\alpha/2}\sqrt{\eta q\kappa(1+\kappa)}\mu}{\sqrt{1+q\eta}\hat{r}^{\alpha/2}}\right){}_1F_2\left(-k,\frac{3}{2}-k;\frac{\mu}{1+\eta};\frac{d^2r^\alpha\kappa(1+\kappa)\mu^2}{\left(d^2-1\right)(1+q\eta)\hat{r}^\alpha}\right) \quad (25)$$

$$N_R(\rho) = \frac{((1+\eta)\mu)^{2\mu-\frac{1}{2}}\rho^{4\mu-1}\sqrt{-\ddot{\psi}(0)}}{\sqrt{2\pi}\eta^\mu 2^{2\mu-2}\Gamma^2(\mu)}\int_0^{\frac{\pi}{2}}\frac{\sin(2\theta)^{2\mu-1}\sqrt{1+\eta-(1-\eta)\cos(2\theta)}}{\exp\left(\left((1+\eta)^2+\left(1-\eta^2\right)\cos(2\theta)\right)\mu\rho^2/(2\eta)\right)}d\theta \quad (33)$$

those remain due to different Doppler frequencies for the in-phase and quadrature waves.

3) PARTICULAR CASE: $d^2 = p/\eta$

An interesting special case for the $\mathrm{LCR_t}$ in (21) can be found when the ratio of the Doppler frequency equates the ratio of η and p, i.e., $d^2 = p/\eta$. After performing the appropriate substitutions, the hypergeometric function can be simplified using [29, Eqn. (15.1.20)], and the summation over the index j can now be solved in closed-form with the help of [29, Eqn. (9.6.10)]. After tedious algebraic manipulations, the $\mathrm{LCR_t}$ yields

$$N_R(r) = \frac{2\sqrt{-\ddot{\psi}(0)}pe^{-\frac{(1+pq)\kappa\mu}{\delta}}}{\sqrt{\pi}\left(\sqrt{\eta}+\sqrt{p}\right)}\left(\frac{\xi\delta}{pq\kappa}\right)^{\frac{\mu}{2}}\left(\frac{\eta}{p}\right)^{\frac{\mu(1-p)}{2(1+p)}}$$
$$\times\sqrt{\frac{q\kappa\mu}{\delta}}\left(\frac{r}{\hat{r}}\right)^{\frac{\alpha\mu}{2}}e^{-\frac{\xi\mu pr^\alpha}{\eta\hat{r}^\alpha}}\sum_{n=0}^{\infty}\left(\left(1-\frac{\eta}{p}\right)\sqrt{\frac{\xi\delta r^\alpha}{q\eta\kappa\hat{r}^\alpha}}\right)^n$$
$$\times L_n^{\frac{\mu}{1+p}-1}\left(\frac{\eta\kappa\mu}{\delta(\eta-p)}\right)I_{\mu+n-1}\left(2p\mu\sqrt{\frac{q\kappa\xi r^\alpha}{\delta\eta\hat{r}^\alpha}}\right). \quad (26)$$

4) PARTICULAR CASE: $d^2 = p/\eta = 1$

By using the limit (23) in (26) with $p \to \eta$ and with the help of [30, Eqn. (5.8.3.4)], after tedious algebraic manipulations, the $\mathrm{LCR_t}$ reduces to

$$N_R(r) = \frac{\sqrt{-\ddot{\psi}(0)}\mu(1+\kappa)^{\mu/2}}{\sqrt{\pi}\exp(\kappa\mu)\kappa^{\frac{\mu-1}{2}}}\left(\frac{r}{\hat{r}}\right)^{\frac{\alpha\mu}{2}}$$
$$\times\exp\left(-\frac{\mu(1+\kappa)r^\alpha}{\hat{r}^\alpha}\right)I_{\mu-1}\left(2\mu\sqrt{\frac{\kappa(1+\kappa)r^\alpha}{\hat{r}^\alpha}}\right). \quad (27)$$

This result represents the $\mathrm{LCR_t}$ for the α-κ-μ when the maximum Doppler shift for the in-phase and quadrature waves are the same.

V. LEVEL CROSSING RATE ANALYSIS IN SPACE-DOMAIN

Thus far we have considered the LCR analysis in the time domain. Although the LCR technique is usually performed in the time domain ($\mathrm{LCR_t}$) [31], it is also possible to extend this concept to the frequency and space domains. The frequency-domain level crossing rate ($\mathrm{LCR_f}$) and space-domain level crossing rate ($\mathrm{LCR_s}$) refer to the average number of times the signal crosses a given amplitude level in the positive or negative direction per frequency or distance unit, respectively [32], [33]. The derivation such an statistics but for these new attributes (space or frequency) follow exactly the same approach as for time. Here, we follow the same approach, but having distance, rather than time, as the crossing attribute, to obtain the $\mathrm{LCR_s}$ statistics, for the various environments, in which, for convenience, ρ is the amplitude level appropriately normalized to the its rms value and $\ddot{\psi}(0)$ is the second derivative with respect to space of the space autocorrelation function at zero. Thus, the $\mathrm{LCR_s}$ for Rayleigh

$$N_R(\rho) = \frac{\rho\sqrt{-\ddot{\psi}(0)}}{\sqrt{\pi}\exp\left(\rho^2\right)}, \quad (28)$$

for Rice (with parameter κ)

$$N_R(\rho) = \frac{\rho\sqrt{-\ddot{\psi}(0)(\kappa+1)}I_0\left(2\rho\sqrt{\kappa(\kappa+1)}\right)}{\sqrt{\pi}\exp(\kappa)\exp((\kappa+1)\rho^2)}, \quad (29)$$

for Nakagami-m (with parameter μ)

$$N_R(\rho) = \frac{\rho^{2\mu-1}\mu^{\mu-\frac{1}{2}}\sqrt{-\ddot{\psi}(0)}}{\sqrt{\pi}\Gamma(\mu)\exp\left(\mu\rho^2\right)}, \quad (30)$$

for α-μ

$$N_R(\rho) = \frac{\rho^{\alpha(\mu-\frac{1}{2})}\mu^{\mu-\frac{1}{2}}\sqrt{-\ddot{\psi}(0)}}{\sqrt{\pi}\Gamma(\mu)\exp\left(\mu\rho^\alpha\right)}. \quad (31)$$

for κ-μ

$$N_R(\rho) = \frac{\sqrt{-\ddot{\psi}(0)\mu\left(1+\kappa\right)^\mu}I_{\mu-1}\left(2\mu\rho\sqrt{\kappa(1+\kappa)}\right)}{\rho^\mu\sqrt{\pi\kappa^{(\mu-1)}}\exp(\mu\kappa)\exp\left(\mu(1+\kappa)\rho^2\right)}, \quad (32)$$

for η-μ the $\mathrm{LCR_s}$ is given in (33), as shown at the top of this page, and finally, for α-η-κ-μ

$$N_R(\rho) = \int_0^{\sqrt{\rho^\alpha}} N_R(\rho, v)dv, \quad (34)$$

where $N_R(\rho, v)$ is given in (35), as shown at the bottom of the next page, d is the imbalance of $\ddot{\psi}(0)$ between in-phase and quadrature components [6, Sec. II]. In (35) we define the following: (i) $\ddot{\psi}(0)$, as the mean of the second derivative with respect to space of the spatial autocorrelation function at zero; (ii) d, as the imbalance of the second derivative with respect to space of the spatial autocorrelation function at zero between in-phase and quadrature components.

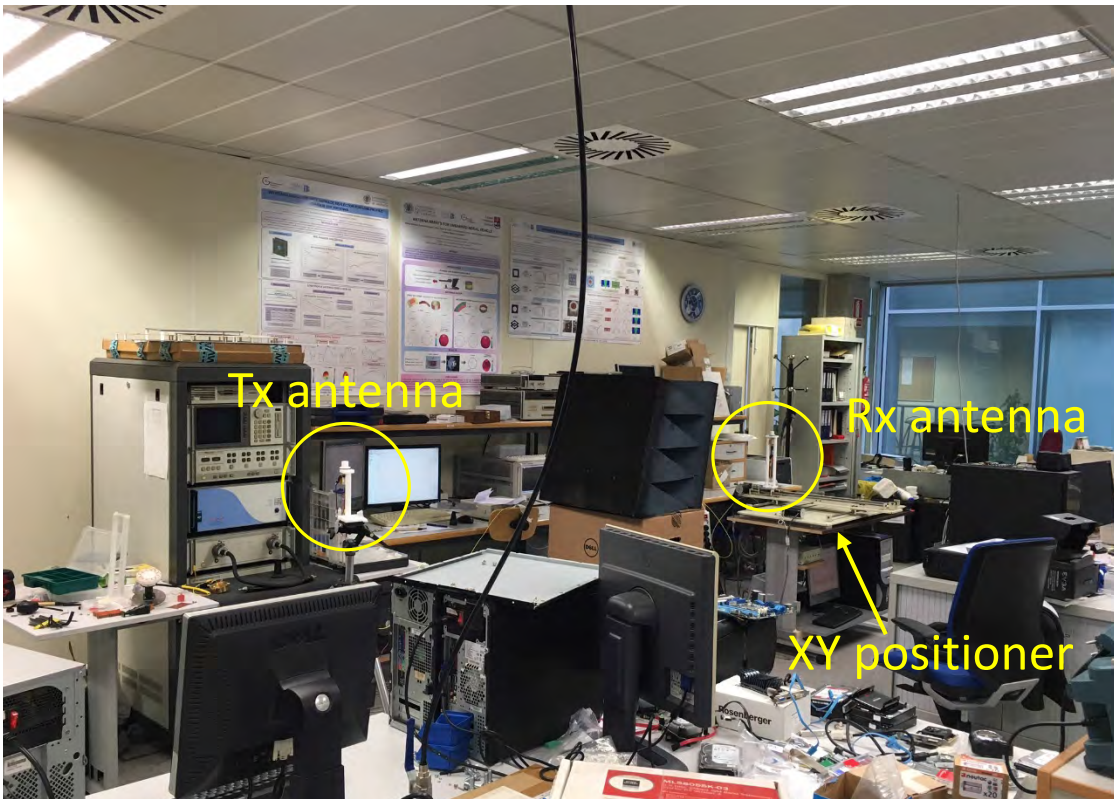

FIGURE 1. View of the propagation environment with the Tx and Rx antennas.

VI. MEASUREMENT CAMPAIGN

A. PROPAGATION ENVIRONMENT

The channel measurements were performed in a laboratory of the iTEAM Research Institute at the Universitat Politècnica de València, Spain. This is an environment characterized by the presence of numerous radiofrequency equipment, electronic devices, metallic cupboards, desks and work tables, among others. These elements interact with the wave fronts producing reflection, diffraction, and scattering mechanisms. These propagation mechanisms render it a rich-multipath environment compared with other indoor environments, such as office or home. Fig. 1 shows a view of the propagation environment. The total dimensions of the laboratory are 13.5-m-long, 7-m-width and 2.6-m-high, and it is integrated into a modern building construction, where both the ceiling and floor are built of reinforced concrete over steel plates, with wood and plasterboards-paneled walls.

$$
\begin{aligned}
N_R(\rho, v) = {} & \frac{4\mu\sqrt{-\ddot{\psi}(0)}(pv^2 + d^2(\rho^\alpha - v^2)\eta)(1+q\eta)\sqrt{(1+\eta)(1+\kappa)\mu p}}{(1+d)(1+p)\sqrt{\pi(\rho^\alpha - v^2)(1+\kappa+\eta(q+\kappa))\eta(1+q(\eta+\kappa+\eta\kappa))(1+p)(pv^2+d^2(\rho^\alpha-v^2)\eta)}} \\
& \times \left(\frac{(1+\eta)\kappa}{1+q\eta}\right)^{\frac{1}{2}(1-\frac{\mu}{1+p})} \left(\frac{q(1+\eta)\kappa}{1+q\eta}\right)^{\frac{1}{2}(1-\frac{p\mu}{1+p})} \left(1+\frac{(1+\eta)\kappa}{1+q\eta}\right)^{\frac{1}{2}(1+\frac{\mu}{1+p})} \left(1+\frac{q(1+\eta)\kappa}{1+q\eta}\right)^{\frac{1}{2}(1+\frac{p\mu}{1+p})} \\
& \times \left(v\sqrt{\frac{(1+\eta)(1+q\eta)(1+\kappa)}{(1+\kappa+\eta(q+\kappa))}}\right)^{\frac{\mu}{1+p}} \left(\sqrt{\frac{\left(\rho^\alpha - v^2\right)(1+\eta)(1+q\eta)(1+\kappa)}{\eta(1+q(\eta+\kappa+\eta\kappa))}}\right)^{\frac{p\mu}{1+p}} \\
& \times \exp\left(-\frac{\mu(1+\eta)\left((1+pq)\eta\kappa + (1+q\eta)\left(p\left(\rho^\alpha - v^2\right) + v^2\eta\right)(1+\kappa)\right)}{\eta(1+p)(1+q\eta)}\right) \\
& \times I_{\frac{\mu}{1+p}-1}\left(\frac{2\mu v(1+\eta)}{(1+p)}\sqrt{\frac{\kappa(1+\kappa)}{(1+q\eta)}}\right) I_{\frac{p\mu}{1+p}-1}\left(\frac{2\mu p(1+\eta)}{(1+p)}\sqrt{\frac{q\kappa\left(\rho^\alpha - v^2\right)(1+\kappa)}{\eta(1+q\eta)}}\right)
\end{aligned} \tag{35}
$$

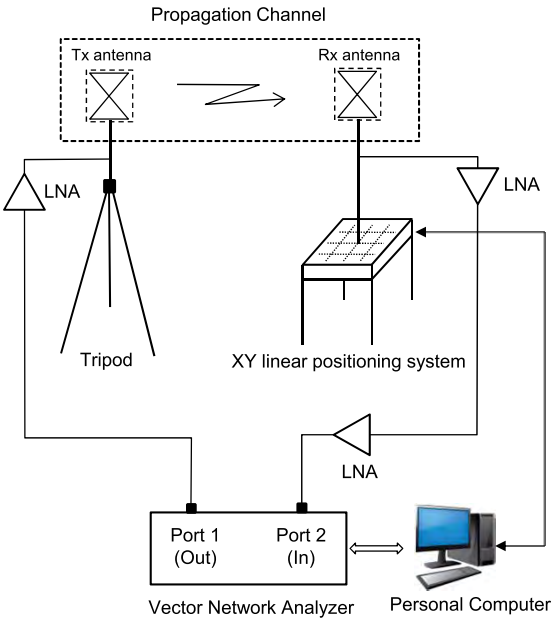

FIGURE 2. Schematic diagram of the channel sounder used in the measurements.

B. MEASUREMENT PROCEDURE AND SETUP

The complex channel transfer function (CTF), denoted by $H(f)$, has been measured using the Keysight N5227A vector network analyzer (VNA). This VNA has 119 dB dynamic range in the target frequency band. Wideband antennas, developed by Q-PAR, have been used at the Tx and Rx sides. These antennas have an omnidirectional radiation pattern in azimuth, linear polarization, and an average gain of 5 dB. Three low noise amplifiers (LNAs), developed by HXI Millimeter Wave Products, with an average gain of 25 dB, one at the Tx side and two at the Rx side, were used to compensate for the propagation losses, which, at these frequencies, are considerably high, increasing the dynamic range in the measurement. In addition, phase-stable cables with an attenuation of 6 dB/m were also used.

The Rx antenna has been located in a XY positioning system, implementing a $N \times M$ (15×750) uniform rectangular array (URA). The separation of the URA elements has been 1 mm. Both, the VNA and the XY positioning systems have been controlled by a personal computer, measuring the CTF at 55 GHz, 60 GHz, and 65 GHz, i.e., 10 GHz of SPAN and 3 frequency points per trace. Before starting the actual measurements, a response calibration of the measurement setup was performed in order to compensate for the attenuation and imperfections of the channel sounder elements. The bandwidth of the intermediate frequency (IF) filter at the VNA was 100 Hz to reduce the power level of the noise floor. A schematic diagram of the channel sounder is illustrated in Fig. 2.

The Tx antenna was mounted on a tripod. Both the Tx and Rx antennas height were 1.44 m above the floor. This height is similar to the average height where many scatterers

TABLE 1. Characteristics of the propagation scenarios.

Scenario	Tx antenna position	Polarization (Tx,Rx)	Propagation
1	Pos1	HV	LoS
2	Pos1	HV	nLoS
3	Pos1	VV	LoS
4	Pos1	VV	nLoS
5	Pos2	HV	LoS
6	Pos2	HV	nLoS
7	Pos2	VV	LoS
8	Pos2	VV	nLoS

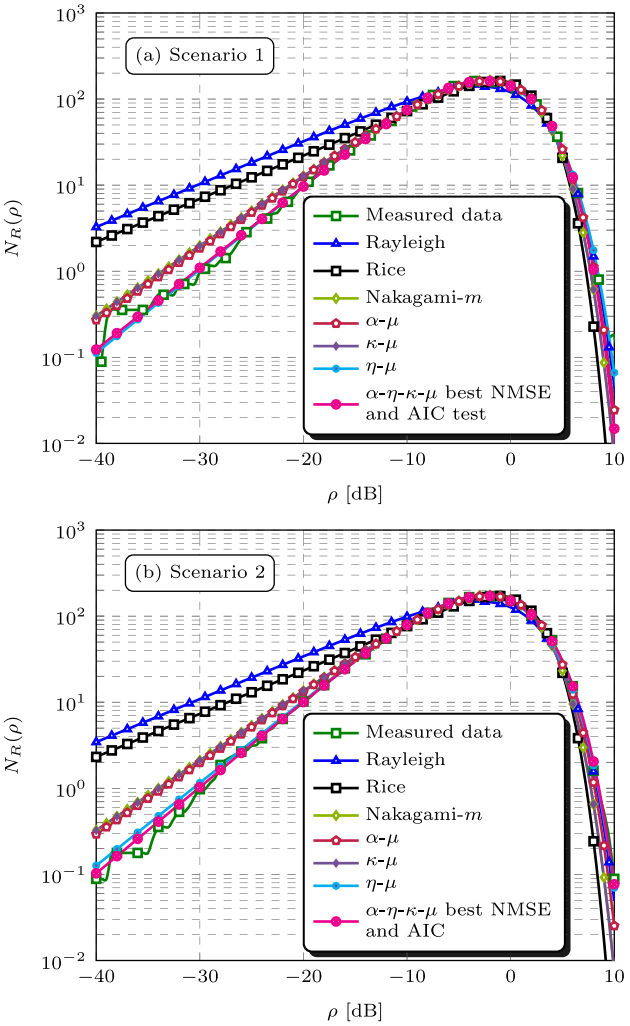

FIGURE 3. LCR_S fitting approach for scenarios 1 (a) and 2 (b) at frequency 60 GHz.

are located in the propagation environment. Two positions for the Tx antenna were considered. In the first position, indicated as Pos1, the Tx-Rx distance was 3.29 m; and in the second position, denoted as Pos2, the Tx-Rx distance was 2.77 m. The channel measurements were collected in different polarizations and propagation conditions,

TABLE 2. $\mathrm{LCR_S}$ fitting results for Scenario 1, Scenario 2 and Scenario 3.

Scenarios	Frequency	Distribution	$\hat{\alpha}$	$\hat{\eta}$	$\hat{\kappa}$	$\hat{\mu}$	$\hat{p}$	$\hat{q}$	$\hat{d}$	$\hat{\psi}[\times 10^3]$	NMSE [dB]	AIC
Scenario 1	55 GHz	Rayleigh	-	-	-	-	-	-	-	-273.85	-13.37	610.96
		Rice	-	-	1.20	-	-	-	-	-674.84	-18.42	472.40
		Nakagami-m	-	-	-	1.28	-	-	-	-385.75	-28.00	205.43
		α-μ	1.86	-	-	1.36	-	-	-	-382.12	-29.14	175.57
		κ-μ	-	-	≈ 0	1.28	-	-	-	-385.79	-28.00	207.43
		η-μ	-	3.12	-	0.69	-	-	-	-368.67	-31.40	112.79
		α-η-κ-μ	1.95	8.11	0.46	1.51	1.63	97.88	0.75	-693.27	$\mathbf{-39.85}$	$\mathbf{-112.67}$
	60 GHz	Rayleigh	-	-	-	-	-	-	-	-334.44	-12.61	576.85
		Rice	-	-	1.29	-	-	-	-	-863.21	-17.63	459.92
		Nakagami-m	-	-	-	1.32	-	-	-	-488.09	-26.74	243.87
		α-μ	1.87	-	-	1.39	-	-	-	-483.75	-27.44	229.05
		κ-μ	-	-	≈ 0	1.32	-	-	-	-487.79	-26.73	245.87
		η-μ	-	0.25	-	0.74	-	-	-	-459.24	-33.70	80.60
		α-η-κ-μ	1.97	2.59	1.26	1.46	0.54	2.19	0.62	-1229.40	$\mathbf{-43.14}$	$\mathbf{-133.12}$
	65 GHz	Rayleigh	-	-	-	-	-	-	-	-353.71	-12.23	610.78
		Rice	-	-	1.34	-	-	-	-	-940.63	-17.50	183.13
		Nakagami-m	-	-	-	1.33	-	-	-	-526.03	-26.66	257.53
		α-μ	1.85	-	-	1.43	-	-	-	-520.40	-27.68	234.21
		κ-μ	-	-	≈ 0	1.33	-	-	-	-526.00	-26.66	259.53
		η-μ	-	0.25	-	0.74	-	-	-	-495.76	-32.26	121.57
		α-η-κ-μ	1.73	1.76	0.87	1.77	0.70	98.89	0.44	-1437.10	$\mathbf{-40.88}$	$\mathbf{-80.90}$
Scenario 2	55 GHz	Rayleigh	-	-	-	-	-	-	-	-303.74	-13.06	564.39
		Rice	-	-	1.22	-	-	-	-	-756.32	-17.76	452.87
		Nakagami-m	-	-	-	1.29	-	-	-	-433.22	-26.63	238.22
		α-μ	1.88	-	-	1.36	-	-	-	-429.60	-27.24	225.54
		κ-μ	-	-	≈ 0	1.29	-	-	-	-433.20	-26.63	240.22
		η-μ	-	0.24	-	0.72	-	-	-	-407.09	-33.83	66.27
		α-η-κ-μ	2.06	0.91	0.80	1.44	2.64	≈ 0	1.01	-703.81	$\mathbf{-39.88}$	$\mathbf{-70.14}$
	60 GHz	Rayleigh	-	-	-	-	-	-	-	-373.21	-12.65	669.56
		Rice	-	-	1.28	-	-	-	-	-959.83	-17.58	534.32
		Nakagami-m	-	-	-	1.31	-	-	-	-543.58	-26.86	275.68
		α-μ	1.88	-	-	1.39	-	-	-	-538.80	-27.52	259.29
		κ-μ	-	-	≈ 0	1.31	-	-	-	-543.60	-26.86	277.68
		η-μ	-	0.25	-	0.73	-	-	-	-512.39	-36.08	20.80
		α-η-κ-μ	1.81	1.70	0.45	1.61	0.72	28.90	0.66	-912.57	$\mathbf{-42.24}$	$\mathbf{-140.77}$
	65 GHz	Rayleigh	-	-	-	-	-	-	-	-444.20	-11.73	708.29
		Rice	-	-	1.47	-	-	-	-	-1259.80	-18.34	529.15
		Nakagami-m	-	-	-	1.37	-	-	-	-686.49	-29.16	232.66
		α-μ	1.83	-	-	1.49	-	-	-	-678.05	-31.83	161.40
		κ-μ	-	-	≈ 0	1.37	-	-	-	-686.75	-29.16	234.66
		η-μ	-	2.70	-	0.73	-	-	-	-663.73	-32.35	147.11
		α-η-κ-μ	1.58	0.53	0.09	1.81	0.86	1.72	49.33	-755.59	$\mathbf{-41.48}$	$\mathbf{-93.00}$
Scenario 3	55 GHz	Rayleigh	-	-	-	-	-	-	-	-77.27	-8.68	470.80
		Rice	-	-	2.26	-	-	-	-	-311.79	-27.55	85.50
		Nakagami-m	-	-	-	1.70	-	-	-	-156.09	-21.74	204.47
		α-μ	1.83	-	-	1.87	-	-	-	-154.32	-22.17	197.80
		κ-μ	-	-	1.40	1.24	-	-	-	-282.95	-33.44	-33.33
		η-μ	-	0.99	-	1.00	-	-	-	-223.37	-15.20	340.47
		α-η-κ-μ	3.19	0.74	1.94	1.01	0.14	7.05	6.50	-221.72	$\mathbf{-39.66}$	$\mathbf{-150.74}$
	60 GHz	Rayleigh	-	-	-	-	-	-	-	-93.03	-8.06	473.58
		Rice	-	-	2.42	-	-	-	-	-398.78	-23.49	180.75
		Nakagami-m	-	-	-	4.79	-	-	-	-200.95	-26.71	119.16
		α-μ	1.91	-	-	1.87	-	-	-	-199.76	-27.03	115.19
		κ-μ	-	-	0.80	1.52	-	-	-	-315.78	-33.87	$\mathbf{-15.73}$
		η-μ	-	1.12×10^6	-	1.79	-	-	-	-200.95	-26.71	121.16
		α-η-κ-μ	1.96	0.97	0.92	1.54	0.95	0.55	9.36	-261.59	$\mathbf{-33.88}$	-5.81
	65 GHz	Rayleigh	-	-	-	-	-	-	-	109.80	-8.16	552.59
		Rice	-	-	2.32	-	-	-	-	-453.00	-26.93	133.45
		Nakagami-m	-	-	-	1.73	-	-	-	-226.99	-22.81	227.49
		α-μ	1.85	-	-	1.88	-	-	-	-224.66	-23.21	220.28
		κ-μ	-	-	1.28	1.30	-	-	-	-401.61	-36.52	-83.16
		η-μ	-	1.09	-	0.99	-	-	-	-306.40	-16.67	369.28
		α-η-κ-μ	3.29	0.63	1.05	1.01	0.14	3.02	19.44	-378.62	$\mathbf{-38.79}$	$\mathbf{-124.74}$

LoS and nLoS. Thus, vertical (V) polarization at the Tx antenna and V polarization at the Rx antenna, indicated as VV, and H polarization at the Tx antenna and V polarization at the Rx antenna, indicated as HV, configurations were considered. Based on the channel propagation conditions, 8 scenarios have been defined. Table 1 summarizes the conditions in which the measurements were collected for each scenario.

C. GOODNESS-OF-FIT TESTS

In order to define which of the theoretical statistical model best fits the practical data, we must specify the goodness-of-fit (GoF) methods used. Practical distributions are obtained empirically through a histogram constructed from field data. Theoretical distributions are found with the respective parameters estimated from the same field data. In the literature there are a number of statistical criteria to define the choice

TABLE 3. LCR$_S$ fitting results for Scenario 4, Scenario 5 and Scenario 6.

Scenarios	Frequency	Distribution	$\hat{\alpha}$	$\hat{\eta}$	$\hat{\kappa}$	$\hat{\mu}$	$\hat{p}$	$\hat{q}$	$\hat{d}$	$\hat{\psi}[\times 10^3]$	NMSE [dB]	AIC
Scenario 4	55 GHz	Rayleigh	-	-	-	-	-	-	-	-330.26	-12.37	663.17
		Rice	-	-	1.34	-	-	-	-	-879.93	-18.06	506.69
		Nakagami-m	-	-	-	1.33	-	-	-	-490.18	-28.54	214.55
		α-μ	1.88	-	-	1.40	-	-	-	-486.17	-29.48	190.45
		κ-μ	-	-	≈ 0	1.33	-	-	-	-490.12	-28.54	216.55
		η-μ	-	0.32	-	0.72	-	-	-	-469.31	-32.81	97.67
		α-η-κ-μ	1.62	0.78	0.02	1.71	1.25	0.02	20.64	-402.58	$\mathbf{-35.41}$	**35.15**
	60 GHz	Rayleigh	-	-	-	-	-	-	-	-375.13	-11.06	556.30
		Rice	-	-	1.60	-	-	-	-	-1136.10	-18.65	402.75
		Nakagami-m	-	-	-	1.42	-	-	-	-607.76	-32.44	120.11
		α-μ	1.89	-	-	1.49	-	-	-	-603.16	-34.55	78.86
		κ-μ	-	-	≈ 0	1.42	-	-	-	-607.74	-32.44	122.11
		η-μ	-	2.16	-	0.74	-	-	-	-595.29	-34.80	73.73
		α-η-κ-μ	2.02	2.73	0.59	1.53	0.98	39.76	1.02	-876.07	$\mathbf{-43.82}$	$\mathbf{-101.08}$
	65 GHz	Rayleigh	-	-	-	-	-	-	-	-407.01	-11.29	640.59
		Rice	-	-	1.54	-	-	-	-	-1195.0	-18.04	479.51
		Nakagami-m	-	-	-	1.40	-	-	-	-646.90	-29.95	191.48
		α-μ	1.90	-	-	1.47	-	-	-	-642.23	-30.87	171.40
		κ-μ	-	-	0.30	1.45	-	-	-	-680.77	-17.92	$\mathbf{-154.66}$
		η-μ	-	2.89	-	0.75	-	-	-	-623.59	-36.37	38.39
		α-η-κ-μ	2.19	0.79	0.56	1.41	2.48	0.13	0.64	-776.15	$\mathbf{-41.58}$	-77.73
Scenario 5	55 GHz	Rayleigh	-	-	-	-	-	-	-	-296.80	-12.36	534.44
		Rice	-	-	1.30	-	-	-	-	-769.17	-16.91	436.96
		Nakagami-m	-	-	-	1.32	-	-	-	-436.74	-25.31	253.21
		α-μ	1.90	-	-	1.38	-	-	-	-433.79	-25.57	249.45
		κ-μ	-	-	≈ 0	1.32	-	-	-	-436.81	-25.31	255.21
		η-μ	-	0.20	-	0.77	-	-	-	-405.62	-37.90	-20.28
		α-η-κ-μ	1.54	0.71	0.63	1.97	1.35	≈ 0	3.90	-1029.40	$\mathbf{-39.46}$	$\mathbf{-44.40}$
	60 GHz	Rayleigh	-	-	-	-	-	-	-	-332.32	-12.81	553.09
		Rice	-	-	1.30	-	-	-	-	-864.70	-18.71	420.63
		Nakagami-m	-	-	-	1.31	-	-	-	-484.07	-29.76	168.75
		α-μ	1.86	-	-	1.40	-	-	-	-479.23	-31.74	125.51
		κ-μ	-	-	≈ 0	1.31	-	-	-	-484.12	-29.76	170.75
		η-μ	-	2.76	-	0.70	-	-	-	-467.23	-34.22	68.96
		α-η-κ-μ	1.65	1.12	0.21	1.65	1.51	≈ 0	3.25	-530.25	$\mathbf{-40.83}$	$\mathbf{-71.65}$
	65 GHz	Rayleigh	-	-	-	-	-	-	-	-364.96	-11.96	650.02
		Rice	-	-	1.41	-	-	-	-	-1005.20	-17.86	498.39
		Nakagami-m	-	-	-	1.35	-	-	-	-554.27	-28.35	225.33
		α-μ	1.87	-	-	1.44	-	-	-	-549.01	-29.48	198.03
		κ-μ	-	-	≈ 0	1.35	-	-	-	-554.15	-28.35	227.33
		η-μ	-	0.32	-	0.73	-	-	-	-530.72	-33.36	97.08
		α-η-κ-μ	1.32	0.93	2.02	2.34	2.12	≈ 0	86.05	-3149.80	$\mathbf{-39.59}$	$\mathbf{-55.01}$
Scenario 6	55 GHz	Rayleigh	-	-	-	-	-	-	-	-312.22	-13.18	511.43
		Rice	-	-	1.24	-	-	-	-	-785.82	-18.60	397.27
		Nakagami-m	-	-	-	1.29	-	-	-	-445.32	-29.33	167.55
		α-μ	1.90	-	-	1.35	-	-	-	-442.07	-30.23	150.35
		κ-μ	-	-	≈ 0	1.29	-	-	-	-445.42	-29.33	169.55
		η-μ	-	0.35	-	0.69	-	-	-	-428.62	-32.78	95.82
		α-η-κ-μ	1.85	1.17	1.19	1.55	0.48	78.94	0.53	-1155.50	$\mathbf{-42.74}$	$\mathbf{-107.54}$
	60 GHz	Rayleigh	-	-	-	-	-	-	-	-336.41	-12.55	560.65
		Rice	-	-	1.34	-	-	-	-	-891.25	-18.54	425.94
		Nakagami-m	-	-	-	1.33	-	-	-	-495.81	-29.06	186.29
		α-μ	1.85	-	-	1.42	-	-	-	-490.37	-31.19	139.72
		κ-μ	-	-	≈ 0	1.33	-	-	-	-495.74	-29.06	188.29
		η-μ	-	2.72	-	0.70	-	-	-	-478.74	-31.94	122.66
		α-η-κ-μ	1.50	1.23	0.95	1.84	1.84	≈ 0	4.54	-1070.30	$\mathbf{-38.59}$	$\mathbf{-18.94}$
	65 GHz	Rayleigh	-	-	-	-	-	-	-	-385.24	-12.76	624.66
		Rice	-	-	1.28	-	-	-	-	-989.76	-17.87	496.18
		Nakagami-m	-	-	-	1.31	-	-	-	-559.33	-28.19	232.41
		α-μ	1.92	-	-	1.36	-	-	-	-556.16	-28.53	225.59
		κ-μ	-	-	≈ 0	1.31	-	-	-	-559.40	-28.19	234.40
		η-μ	-	0.30	-	0.71	-	-	-	-532.21	-36.15	30.91
		α-η-κ-μ	1.43	1.09	1.14	1.96	0.66	72.41	≈ 0	-1421.50	$\mathbf{-40.33}$	$\mathbf{-65.83}$

between one or another model, each of which with specific characteristics [34]–[39].

In the analyses conducted here, two different figures of merit or criteria, borrowed from the probability theory, are used, namely NMSE, and Akaike information criterion (AIC). The NMSE is used for analyses in which the focus is to compare the empirical LCR$_S$ and the theoretical ones in order to quantify the LCR$_S$s dissimilarity (mean distance). The AIC is used to compare empirical and theoretical statistics considering dissimilarity, quantity of samples, and number of parameters of the formulation. In these two statistical tests aforementioned, objective figures of merit are obtained that can be used to evaluate the GoF between empirical and theoretical statistics. In NMSE and AIC tests, the chosen statistics is the one with the lowest value. Because NMSE and AIC statistical tests use different approaches, the conclusions

TABLE 4. LCR_S fitting results for Scenario 7 and Scenario 8.

Scenarios	Frequency	Distribution	$\hat{\alpha}$	$\hat{\eta}$	$\hat{\kappa}$	$\hat{\mu}$	$\hat{p}$	$\hat{q}$	$\hat{d}$	$\hat{\tilde{\psi}}[\times 10^3]$	NMSE [dB]	AIC
Scenario 7	55 GHz	Rayleigh	-	-	-	-	-	-	-	-150.51	-5.13	585.85
		Rice	-	-	4.12	-	-	-	-	-1062.80	-27.68	157.03
		Nakagami-m	-	-	-	2.67	-	-	-	-534.20	-26.20	185.16
		α-μ	2.01	-	-	2.66	-	-	-	-534.48	-26.21	187.12
		κ-μ	-	-	1.26	1.92	-	-	-	-890.18	-33.16	$\mathbf{-54.23}$
		η-μ	-	0.99	-	1.27	-	-	-	-482.68	-23.92	230.84
		α-η-κ-μ	2.04	1.32	1.85	1.65	1.52	0.61	24.82	-611.68	$\mathbf{-39.29}$	-52.92
	60 GHz	Rayleigh	-	-	-	-	-	-	-	-169.17	-4.01	522.35
		Rice	-	-	5.67	-	-	-	-	-1625.20	-27.98	154.57
		Nakagami-m	-	-	-	3.49	-	-	-	-819.43	-27.07	168.52
		α-μ	2.04	-	-	3.39	-	-	-	-821.25	-27.13	169.70
		κ-μ	-	-	1.24	2.48	-	-	-	-1334.70	-31.27	105.83
		η-μ	-	1.06	-	1.66	-	-	-	-741.58	-24.47	210.76
		α-η-κ-μ	2.00	2.12	6.88	0.92	3.65	0.98	13.35	-837.50	$\mathbf{-37.41}$	$\mathbf{21.03}$
	65 GHz	Rayleigh	-	-	-	-	-	-	-	-175.07	-4.48	655.34
		Rice	-	-	4.90	-	-	-	-	-1463.20	-26.63	203.31
		Nakagami-m	-	-	-	3.08	-	-	-	-737.31	-27.23	191.01
		α-μ	2.08	-	-	2.93	-	-	-	-740.67	-27.43	188.93
		κ-μ	-	-	1.02	2.37	-	-	-	-1165.80	-30.56	124.81
		η-μ	-	0.98	-	1.49	-	-	-	-685.28	-25.58	226.81
		α-η-κ-μ	2.02	2.63	2.69	1.32	13.34	12.60	7.61	-536.66	$\mathbf{-41.11}$	$\mathbf{-81.40}$
Scenario 8	55 GHz	Rayleigh	-	-	-	-	-	-	-	-332.60	-13.41	674.25
		Rice	-	-	1.16	-	-	-	-	-1038.40	-17.40	563.03
		Nakagami-m	-	-	-	1.28	-	-	-	-605.44	-26.06	317.90
		α-μ	2.00	-	-	1.28	-	-	-	-605.29	-26.06	319.82
		κ-μ	-	-	≈ 0	1.28	-	-	-	-605.53	-26.06	319.90
		η-μ	-	0.23	-	0.72	-	-	-	-566.07	-36.49	24.46
		α-η-κ-μ	1.56	3.05	≈ 0	1.78	1.56	99.09	≈ 0	-1018.60	$\mathbf{-38.56}$	$\mathbf{24.17}$
	60 GHz	Rayleigh	-	-	-	-	-	-	-	-453.33	-11.11	708.38
		Rice	-	-	1.58	-	-	-	-	-1361.70	-18.60	512.07
		Nakagami-m	-	-	-	1.41	-	-	-	-729.22	-29.18	231.84
		α-μ	1.80	-	-	1.56	-	-	-	-718.71	-34.32	97.84
		κ-μ	-	-	0.15	1.40	-	-	-	-619.26	-17.01	232.67
		η-μ	-	2.27	-	0.74	-	-	-	-712.48	-30.39	201.97
		α-η-κ-μ	1.51	1.19	0.56	1.92	1.39	≈ 0	24.59	-869.67	$\mathbf{-39.79}$	$\mathbf{-36.98}$
	65 GHz	Rayleigh	-	-	-	-	-	-	-	-523.89	-11.13	639.01
		Rice	-	-	≈ 0	-	-	-	-	-287.56	-13.23	593.12
		Nakagami-m	-	-	-	1.41	-	-	-	-841.22	-28.88	236.45
		α-μ	1.81	-	-	1.55	-	-	-	$-829..56$	-32.42	157.81
		κ-μ	-	-	≈ 0	1.41	-	-	-	-841.22	-28.88	238.44
		η-μ	-	2.68	-	0.75	-	-	-	-814.48	-31.61	176.23
		α-η-κ-μ	1.60	2.25	0.10	1.85	3.19	≈ 0	12.48	-451.26	$\mathbf{-42.14}$	$\mathbf{-53.77}$

drawn from them will not necessarily be the same, that is the chosen statistics in one test may not coincide with the one in the others.

VII. RESULTS

In this subsection, the adherence of the theoretical LCR_S curves to the empirical LCR_S ones in all eight scenarios described in Subsections VI-A and VI-B at frequencies 55 GHz, 60 GHz and 65 GHz is assessed.[2]

For the analysis conducted here, and for each one of the frequencies and for all eight scenarios, the parameters of the target fading models (i.e., Rayleigh, Rice, Nakagami-m, α-μ, κ-μ, η-μ, and α-η-κ-μ) have been estimated. Several built-in functions are available within Matlab that can be used for parameter estimation purposes. In our case, the Matlab least-square-error based function has been chosen, namely `lsqcurvefit`. For fairness, the same method is utilized for all distributions with the same starting point. More details on `lsqcurvefit` function can be found at [40]. Having the parameters estimated, then the NMSE as well as the AIC metrics are found aiming to find the best fit for each evaluated scenarios.

Tables 2, 3 and 4 summarize the parameter estimates and the values of NMSE, in dB, and AIC. From the mentioned tables, it can be seen that in all evaluated scenarios the best-fitting performance (highlighted in bold) has been achieved by the more general fading models. The NMSE and AIC criteria do not necessarily agree with each other. Whereas through the first criterion for 24 out of 24 tests the best-fittings have been achieved by the most general fading distributions, through the second one these figures are 21 out of 24.

The effect of the polarization combination on the short-term fading distribution can be inferred from the estimated parameters in Scenario 1 and Scenario 3 with LoS condition corresponding to the same Tx and Rx antenna positions and polarization combinations HV and VV, respectively, as it is shown in Table 2. The estimated κ parameters of the κ-μ distribution for the frequencies of 55, 60 and 65 GHz are approximately zero for HV and 1.40, 0.80 and 1.28 for VV. Using HV combination the LoS contribution substantially

[2]Because the AFD is a direct application of (18), in the plots, we shall explore only the LCR.

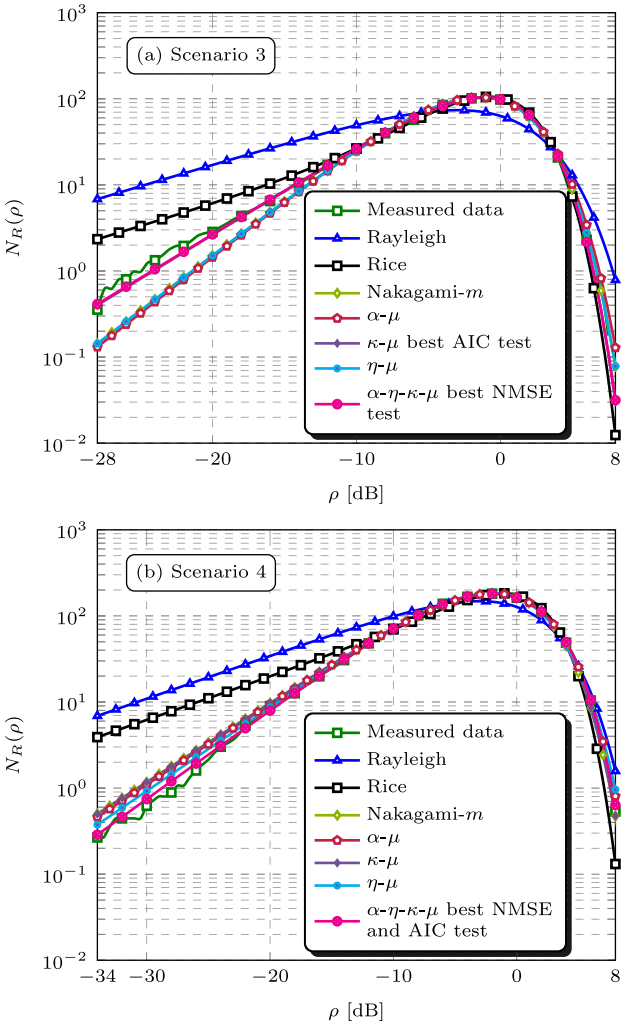

FIGURE 4. LCR_S fitting approach for Scenarios 3 (a) and 4 (b) at frequency 60 GHz.

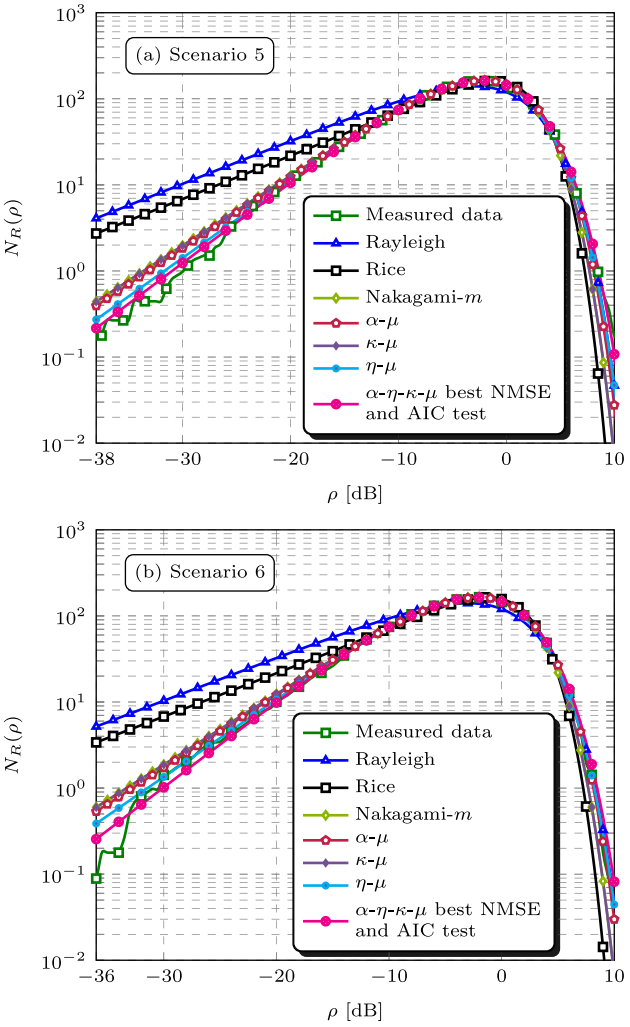

FIGURE 5. LCR_S fitting approach for Scenarios 5 (a) and 6 (b) at frequency 60 GHz.

decreases with a significantly lower level given by the cross-polarization component of both Tx and Rx antennas. Nevertheless, in the case of HV, the diffuse component does not decrease as the LoS dominant component diminishes. This is due to the fact that the reflected and scattered components suffer polarization changes in the process of reflection and scattering and thus the overall diffuse component in HV is not significantly lower than in VV. Therefore, the κ parameter is expected to be smaller in HV than in VV. Particularly, in the case of HV polarization for the Scenario 1, the estimated values of the κ parameter of the κ-μ distribution are very close to 0 and consequently the short-term fading distribution can be approximated by a Nakagami-m distribution where the dominant component is negligible compared to the diffuse component. The same conclusions can be drawn by analyzing Scenario 5 and Scenario 7.

If we consider the NMSE metric in all three frequencies in the eight scenarios, the best performance, has been achieved by the α-η-κ-μ fading model, an already expected result, since it has more parameters and thus is more flexible. Considering the AIC metric, in most scenarios the best results have also been obtained by the α-η-κ-μ. In the exception scenarios, despite providing a better fit considering the NMSE metric, the α-η-κ-μ model did not obtain the best performance in the AIC test. This is justifiable, since the AIC test penalizes models with more parameters, which is the case of the α-η-κ-μ (7 parameters). In fact, in Scenario 3, polarization VV with LoS condition, the model that provided the best result in the AIC test has been the κ-μ (2 parameters), this way, for Scenario 3, constituting the best model considering a compromise between fit and complexity.

Consider next the LCR_S fitting process analysis. Figs. 3, 4, 5 and 6 graph the theoretical LCR_S curves plotted alongside the empirical one for all scenarios at frequency 60 GHz as a function of the normalized enveloped ρ in dB.

Analyzing the results presented in these figures, it is possible to verify that, for Scenarios 1 and 2, presented at Fig. 3, with the exceptions of Rayleigh and Rice distributions, all the other distributions match rather well the empirical LCR_S. However, if we look carefully only at the extremely lower

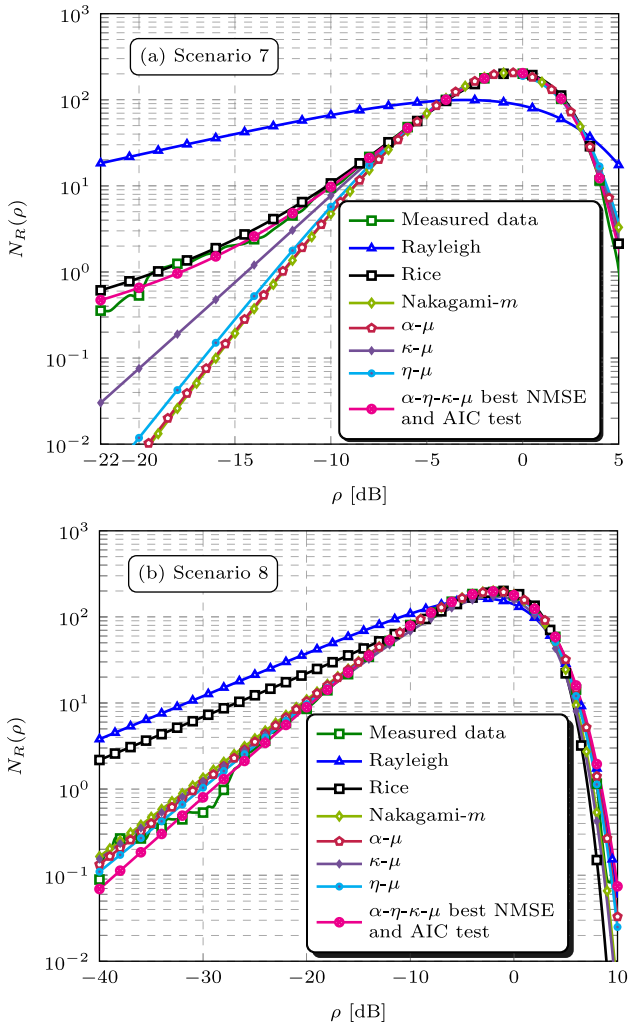

FIGURE 6. LCR_s fitting approach for Scenarios 7 (a) and 8 (b) at frequency 60 GHz.

tail portion of the plots, i.e., for substantially small ρ, the α-η-κ-μ and η-μ yield a better adherence. In fact, the best-fitting considering the NMSE and AIC metrics is found for α-η-κ-μ distribution in both scenarios. Note that in Scenario 1, although we are in LoS conditions, the Rice and κ-μ distributions, known to perform well in this type of situation, did not present good results. This can be credited to the polarization combination HV which substantially decreases the contribution of the dominant component. For Scenario 3, presented at Fig. 4(a), with exception of Rayleigh, all the other fading models achieved a reasonable fitting. Note, however that in this scenario, differently from what happened in Scenario 1, the κ-μ distribution presented an excellent result, since the direct components of received signal is not degraded due to polarization combination VV. In this case, the best-fitting considering the NMSE and AIC metrics has been obtained by the α-η-κ-μ and κ-μ, respectively. For Scenario 4, shown in Fig. 4(b), since we are in nLoS conditions, all models capable of modeling multipath clusters have achieved a very good fitting. In this specific case, the best result has been achieved by α-η-κ-μ in both test metrics. For Scenarios 5 and 6, presented at Fig. 5, we have very similar results as those presented in Scenarios 1 and 2, where, with the exception of the Rayleigh and Rice distributions, all other distributions presented a good fit, being the best of them achieved by the most generalized fading model in both cases. For Scenario 7, presented at Fig. 6(a), we have a very interesting result, where it is possible to verify the excellent fitting made by α-η-κ-μ that makes changes of concavity to follow the trend of the empirical curve. Models capable of modeling dominant components have reached a better fit than those that do not have this skill, since the transmission in this scenario is performed in a LoS situation. Finally, for Scenario 8, similar to Scenario 4, the models with skill of modeling multipath clusters have obtained a better adjustment. In fact, the best-fitting considering the NMSE and AIC metrics is found again for α-η-κ-μ distribution in this last scenario.

VIII. CONCLUSIONS

The scarcity of information on channel modeling in the mmWave band, e.g. short-term fading characterization, has motivated researchers to conduct measurement campaigns to better understand the behavior of the channel. This paper contributes in this direction investigating the higher-order statistics, more specifically the level crossing rate and average fade duration, through field measurements. With such a purpose, an extensive field measurement campaign in the mmWave band has been conducted in an indoor environment. The frequencies ranged from 55 GHz to 65 GHz, and the propagation conditions included LoS and nLoS, with combinations of horizontal and vertical polarizations at both transmitter and receiver.

In addition, the theory concerning the α-η-κ-μ has been further advanced with the derivation of new expressions concerning its higher-order statistics. For these, an envelope-based approach has been used that facilitates the computation of the expressions as compared to their counterparts available in the literature, for which the knowledge of the phase is required. Most interestingly, exact formulations for LCR_t and AFD_t has been attained. Finally, a formulation for the LCR_t in series expansion has also been presented.

The models that best fit the experimental data have been chosen using two figures of merit, namely NMSE and AIC. Analyzing the results of the tests, it has been possible to verify that the most general model, namely the α-η-κ-μ, provides the smallest NMSE estimation error in all 24 scenarios analyzed. For the AIC metric, this same model performed better in 21 out of 24 scenarios. From these results, it is possible to conclude that the most general model will most of the time provide a better fitting performance as compared to the simpler ones. Although this performance improvement comes accompanied by an increase of a mathematical complexity, it has been verified through the AIC metric that, in most cases, this inconvenience is rewarded by a significant gain in the quality of its adjustment. On the other hand, if mathematical

$$N_R(r) = \frac{2^{\frac{1}{2}(3-\mu_x-\mu_y)}\sqrt{-\ddot{\psi}_x(0)}r^{\alpha/2}}{\sqrt{\pi}\sigma_x^{\mu_x-1}\sigma_y^{\mu_y}} e^{-\frac{1}{2}\left(\frac{r^\alpha+\lambda_x^2}{\sigma_x^2}+\frac{\lambda_y^2}{\sigma_y^2}\right)} \sum_{i=0}^{\infty}\sum_{j=0}^{\infty}\sum_{k=0}^{\infty} \frac{(-1)^i}{i!j!k!\Gamma\left(j+\frac{\mu_x}{2}\right)\Gamma\left(k+\frac{\mu_y}{2}\right)} \left(\frac{1}{2}\left(\frac{1}{\sigma_y^2}-\frac{1}{\sigma_x^2}\right)\right)^i \times \left(\frac{\lambda_x}{2\sigma_x^2}\right)^{2j}\left(\frac{\lambda_y}{2\sigma_y^2}\right)^{2k} \int_0^{\sqrt{r^\alpha}} \sqrt{1+\frac{v^2}{r^\alpha}\left(\frac{\ddot{\psi}_y(0)\sigma_y^2}{\ddot{\psi}_x(0)\sigma_x^2}-1\right)} v^{\mu_y+2(i+k)-1}\left(r^\alpha-v^2\right)^{\frac{\mu_x}{2}+j-1} dv \tag{36}$$

$$N_R(r) = \frac{2^{\frac{1-\mu_x-\mu_y}{2}}\sqrt{-\ddot{\psi}_x(0)}}{\sqrt{\pi}\sigma_x^{\mu_x-1}\sigma_y^{\mu_y}} r^{\frac{\alpha}{2}(\mu_x+\mu_y-1)} e^{-\frac{1}{2}\left(\frac{r^\alpha+\lambda_x^2}{\sigma_x^2}+\frac{\lambda_y^2}{\sigma_y^2}\right)} \sum_{i=0}^{\infty}\sum_{j=0}^{\infty}\sum_{k=0}^{\infty} \frac{(-1)^i\Gamma\left(i+k+\frac{\mu_y}{2}\right)}{i!j!k!\Gamma\left(k+\frac{\mu_y}{2}\right)} \left(\frac{r^\alpha}{2}\left(\frac{1}{\sigma_y^2}-\frac{1}{\sigma_x^2}\right)\right)^i \times \left(\frac{r^{\alpha/2}\lambda_x}{2\sigma_x^2}\right)^{2j}\left(\frac{r^{\alpha/2}\lambda_y}{2\sigma_y^2}\right)^{2k} {}_2\tilde{F}_1\left(-\frac{1}{2}, i+k+\frac{\mu_y}{2}; i+j+k+\frac{\mu_x+\mu_y}{2}; 1-\frac{\ddot{\psi}_y(0)\sigma_y^2}{\ddot{\psi}_x(0)\sigma_x^2}\right) \tag{37}$$

burden is to be avoided, the less, but still, general models, namely α-μ, η-μ, and κ-μ can be used to yield excellent results. All in all, it must be said the available fading models can be satisfactorily used in this harsh mmWave band.

APPENDIX
NOVEL LCR POWER SERIES -

Let's consider the integral-form for the $\mathrm{LCR_t}$ given in (17). The proof begins by replacing the modified Bessel and the exponential functions therein in terms of their respective power series using [29, Eqns. (9.6.10) and (4.2.1)], respectively. After some tedious algebraic manipulations the $\mathrm{LCR_t}$ is given as a triple series as in (36), as shown at the top of this page. The inner integral can be solved with the help of [41, Eqn. (2.2.6.1)], yielding (37), as shown at the top of this page. At this point, we can consider the summation over the infinite triangle $i = n - k$. After replacing the index i and isolating the sum over the index k, the inner summation is solved as

$$\sum_{k=0}^{n} \frac{(-1)^{-k}2^{-k}}{k!(n-k)!\Gamma\left(k+\frac{\mu_y}{2}\right)} \left(\frac{\lambda_y^2\sigma_x^2}{\left(\sigma_x^2-\sigma_y^2\right)\sigma_y^2}\right)^k = \frac{1}{\Gamma\left(n+\frac{\mu_y}{2}\right)} L_n^{\frac{\mu_y}{2}-1}\left(\frac{\lambda_y^2\sigma_x^2}{2\left(\sigma_x^2-\sigma_y^2\right)\sigma_y^2}\right). \tag{38}$$

Using this identity in (37), the $\mathrm{LCR_t}$ is obtained as a double infinite series given in terms of the Raw parametrization of the α-η-κ-μ fading model. To complete the proof what remains is to perform the adequate parameter substitutions between the Raw and Global parameterizations, which are given in [25]. After some tedious algebraic manipulations (21) yields.

REFERENCES

[1] P. Newman, "How Internet of Things technology growth is reaching mainstream companies and consumers," Bus. Insider, New York, NY, USA, Tech. Rep., Jan. 2019. Accessed: Feb. 12, 2019. [Online]. Available: https://www.businessinsider.com/internet-of-things-report

[2] C. F. Kerry and J. Karsten, "Gauging investment in self-driving cars," Brookings Inst., Washington, DC, USA, Tech. Rep., Oct. 2017. Accessed: Feb. 10, 2019. [Online]. Available: https://www.brookings.edu/research/gauging-investment-in-self-driving-cars/

[3] R. Dagar, S. Som, and S. K. Khatri, "Smart farming—IoT in agriculture," in *Proc. Int. Conf. Inventive Res. Comput. Appl. (ICIRCA)*, Jul. 2018, pp. 1052–1056.

[4] M. Shafi, A. F. Molisch, P. J. Smith, T. Haustein, P. Zhu, P. De Silva, F. Tufvesson, A. Benjebbour, and G. Wunder, "5G: A tutorial overview of standards, trials, challenges, deployment, and practice," *IEEE J. Sel. Areas Commun.*, vol. 35, no. 6, pp. 1201–1221, Jun. 2017.

[5] *Technical Specification Group Radio Access Network; NR; User Equipment (UE) Radio Transmission and Reception*, document 3GPP TS 38.101-2 V15.5.0, Apr. 2019. [Online]. Available: https://www.3gpp.org/ftp/Specs/archive/38_series/38.101-2/

[6] A. A. dos Anjos, T. R. R. Marins, R. A. A. de Souza, and M. D. Yacoub, "Higher order statistics for the α-η-κ-μ fading model," *IEEE Trans. Antennas Propag.*, vol. 66, no. 6, pp. 3002–3016, Jun. 2018.

[7] T. Zwick, T. J. Beukema, and H. Nam, "Wideband channel sounder with measurements and model for the 60 GHz indoor radio channel," *IEEE Trans. Veh. Technol.*, vol. 54, no. 4, pp. 1266–1277, Jul. 2005.

[8] H. Xu, V. Kukshya, and T. S. Rappaport, "Spatial and temporal characteristics of 60-GHz indoor channels," *IEEE J. Sel. Areas Commun.*, vol. 20, no. 3, pp. 620–630, Apr. 2002.

[9] C. R. Anderson and T. S. Rappaport, "In-building wideband partition loss measurements at 2.5 and 60 GHz," *IEEE Trans. Wireless Commun.*, vol. 3, no. 3, pp. 922–928, May 2004.

[10] P. F. M. Smulders, "Statistical characterization of 60-GHz indoor radio channels," *IEEE Trans. Antennas Propag.*, vol. 57, no. 10, pp. 2820–2829, Oct. 2009.

[11] H. J. Thomas, R. S. Cole, and G. L. Siqueira, "An experimental study of the propagation of 55 GHz millimeter waves in an urban mobile radio environment," *IEEE Trans. Veh. Technol.*, vol. 43, no. 1, pp. 140–146, Feb. 1994.

[12] M. Kyro, K. Haneda, J. Simola, K. I. Takizawa, H. Hagiwara, and P. Vainikainen, "Statistical channel models for 60 GHz radio propagation in hospital environments," *IEEE Trans. Antennas Propag.*, vol. 60, no. 3, pp. 1569–1577, Mar. 2012.

[13] T. S. Rappaport, S. Sun, R. Mayzus, H. Zhao, Y. Azar, K. Wang, G. N. Wong, J. K. Schulz, M. Samimi, and F. Gutierrez, "Millimeter wave mobile communications for 5G cellular: It will work!" *IEEE Access*, vol. 1, pp. 335–349, May 2013.

[14] S. Hur, S. Baek, B. Kim, Y. Chang, A. F. Molisch, T. S. Rappaport, K. Haneda, and J. Park, "Proposal on millimeter-wave channel modeling for 5G cellular system," *IEEE J. Sel. Topics Signal Process.*, vol. 10, no. 3, pp. 454–469, Apr. 2016.

[15] K. Haneda, J. Järveläinen, A. Karttunen, M. Kyrö, and J. Putkonen, "Indoor short-range radio propagation measurements at 60 and 70 GHz," in *Proc. 8th Eur. Conf. Antennas Propag. (EuCAP)*, Apr. 2014, pp. 634–638.

[16] M.-S. Choi, G. Grosskopf, and D. Rohde, "Statistical characteristics of 60 GHz wideband indoor propagation channel," in *Proc. IEEE 16th Int. Symp. Pers., Indoor Mobile Radio Commun.*, vol. 1, Sep. 2005, pp. 599–603.

[17] M. K. Samimi, G. R. MacCartney, S. Sun, and T. S. Rappaport, "28 GHz millimeter-wave ultrawideband small-scale fading models in wireless channels," in *Proc. IEEE 83rd Veh. Technol. Conf. (VTC Spring)*, May 2016, pp. 1–6.

[18] T. Mavridis, L. Petrillo, J. Sarrazin, A. Benlarbi-Delaï, and P. De Doncker, "Near-body shadowing analysis at 60 GHz," *IEEE Trans. Antennas Propag.*, vol. 63, no. 10, pp. 4505–4511, Oct. 2015.

[19] J. Reig, M.-T. Martínez-Inglés, L. Rubio, V.-M. Rodrigo-Peñarrocha, and J.-M. Molina-García-Pardo, "Fading evaluation in the 60 GHz band in line-of-sight conditions," *Int. J. Antennas Propag.*, vol. 2014, Aug. 2014, Art. no. 984102.

[20] M. D. Yacoub, "The α-μ distribution: A physical fading model for the Stacy distribution," *IEEE Trans. Veh. Technol.*, vol. 56, no. 1, pp. 27–34, Jan. 2007.

[21] M. Yacoub, "The κ-μ distribution and the η-μ distribution," *IEEE Antennas Propag. Mag.*, vol. 49, no. 1, pp. 68–81, Feb. 2007.

[22] G. Fraidenraich and M. D. Yacoub, "The α-η-μ and α-κ-μ fading distributions," *Proc. IEEE 9th Int. Symp. Spread Spectrum Techn. Appl.*, vol. 49, no. 1, Aug. 2006, pp. 16–20.

[23] J. Blumenstein, T. Mikulasek, T. Zemen, C. Mecklenbrauker, R. Marsalek, and A. Prokes, "In-vehicle mm-wave channel model and measurement," in *Proc. IEEE 80th Veh. Technol. Conf. (VTC-Fall)*, Sep. 2014, pp. 1–5.

[24] J. Blumenstein, A. Prokes, A. Chandra, T. Mikulasek, R. Marsalek, T. Zemen, and C. Mecklenbräuker, "In-vehicle channel measurement, characterization, and spatial consistency comparison of 30–11 GHz and 55–65 GHz frequency bands," *IEEE Trans. Veh. Technol.*, vol. 66, no. 5, pp. 3526–3537, May 2017.

[25] M. D. Yacoub, "The α-η-κ-μ fading model," *IEEE Trans. Antennas Propag.*, vol. 64, no. 8, pp. 3597–3610, Aug. 2016.

[26] U. S. Dias and M. D. Yacoub, "The κ-μ phase-envelope joint distribution," *IEEE Trans. Commun.*, vol. 58, no. 1, pp. 40–45, Jan. 2010.

[27] I. B. G. Pôrto and M. D. Yacoub, "On the phase statistics of the κ-μ process," *IEEE Trans. Wireless Commun.*, vol. 15, no. 7, pp. 4732–4744, Jul. 2016.

[28] I. Gradshteyn and I. Ryzhik, *Table of Integrals, Series, and Products*. New York, NY, USA: Academic, 1980.

[29] M. Abramowitz, *Handbook of Mathematical Functions: With Formulas, Graphs, and Mathematical Tables*. New York, NY, USA: Dover, 1974.

[30] A. P. Prudnikov, Y. A. Brychkov, and O. I. Marichev, *Integrals and Series: Special Functions*, vol. 2. New York, NY, USA: Gordon and Breach Science Publishers, 1986.

[31] S. Cotton and W. G. Scanlon, "Higher-order statistics for κ-μ distribution," *Electron. Lett.*, vol. 43, no. 22, pp. 1–2, Feb. 2007.

[32] R. Zhang, Z. Zhong, Y. Zhang, S. Lu, and L. Cai, "Measurement and analytical study of the correlation properties of subchannel fading for noncontiguous carrier aggregation," *IEEE Trans. Veh. Technol.*, vol. 63, no. 9, pp. 4165–4177, Nov. 2014.

[33] T. R. R. Marins, A. A. dos Anjos, V. M. R. Penarrocha, L. Rubio, J. Reig, R. A. A. de Souza, and M. D. Yacoub, "Fading evaluation in the mm-wave band," *IEEE Trans. Commun.*, to be published.

[34] P. Chen, T. J. Wu, and J. Yang, "A comparative study of model selection criteria for the number of signals," *IET Radar, Sonar Navigat.*, vol. 2, no. 3, pp. 180–188, Jun. 2008.

[35] A. Mariani, A. Giorgetti, and M. Chiani, "Model order selection based on information theoretic criteria: Design of the penalty," *IEEE Trans. Signal Process.*, vol. 63, no. 11, pp. 2779–2789, Jun. 2015.

[36] A. Seghouane, "The Akaike information criterion with parameter uncertainty," in *Proc. 4th IEEE Workshop Sensor Array Multichannel Process.*, Jul. 2006, pp. 430–434.

[37] J. Ding, V. Tarokh, and Y. Yang, "Model selection techniques: An overview," *IEEE Signal Process. Mag.*, vol. 35, no. 6, pp. 16–34, Nov. 2018.

[38] J. K. Nielsen, M. G. Christensen, and S. H. Jensen, "Bayesian model comparison and the BIC for regression models," in *Proc. IEEE Int. Conf. Acoust., Speech Signal Process.*, May 2013, pp. 6362–6366.

[39] P. Stoica and Y. Selen, "Model-order selection: A review of information criterion rules," *IEEE Signal Process. Mag.*, vol. 21, no. 4, pp. 36–47, Jul. 2004.

[40] MathWorks. *Lscurvefit Function*. Accessed: Oct. 5, 2018. [Online]. Available: https://www.mathworks.com/help/optim/ug/lsqcurvefit.html

[41] A. P. Prudnikov, Y. A. Bryčkov, and O. I. Maričev, *Integrals and Series: Elementary Functions*, vol. 1, 2nd ed. Moscow, Russia: Fizmatlit, 2002.

ANDRÉ ANTÔNIO DOS ANJOS was born in Brazil, in 1986. He received the B.Sc. degree in electrical engineering and the M.Sc. degree in telecommunications from the National Institute of Telecommunications (INATEL), Brazil, in 2009 and 2012, respectively. He is currently pursuing the Ph.D. degree with the University of Campinas (UNICAMP), Campinas, Brazil. He is also an Engineer with the INATEL Competence Center (ICC). His general research interests include wireless communications, fading channel modeling and simulation, non-linear systems, and spectrum sensing.

TIAGO REIS RUFINO MARINS was born in Brazil, in 1983. He received the B.Sc. degree in electrical engineering and the M.Sc. degree in telecommunications from the National Institute of Telecommunications (INATEL), Brazil, in 2008 and 2012, respectively. He is currently pursuing the Ph.D. degree with the University of Campinas (UNICAMP), Campinas, Brazil. He is also a Researcher with the Radiocommunication Reference Center (RRC), INATEL. His fields of interest include digital communications, channel coding, wireless communications, and channel modeling, which is the topic he has published scientific papers.

CARLOS RAFAEL NOGUEIRA DA SILVA was born in Brazil, in 1986. He received the B.S. degree in electrical engineering from the Federal University of Itajubá, Brazil, in 2010, the M.S. degree in electrical engineering from the National Institute of Telecommunications, in 2012, and the Ph.D. degree from the School of Electrical and Computer Engineering, State University of Campinas, UNICAMP, in 2018, where he is currently holding a Postdoctoral FAPESP Scholarship. His research interests include wireless channel modeling, spectrum sensing, cognitive radio, composite channel characterization and applications, and wireless communications in general.

VICENT MIQUEL RODRIGO PEÑARROCHA was born in Valencia, Spain, in 1966. He received the M.S. degree in telecommunications engineering from the Universidad Politécnica de Madrid, Spain, in 1990, and the Ph.D. degree in telecommunications engineering from the Universitat Politècnica de València, Spain, in 2003. He joined the Departamento de Comunicaciones, Universitat Politècnica de València, in 1991, as a Lecturer. His current interests include radiowave propagation, antenna measurements, instrumentation, virtual instrumentation and laboratories, and any educational activity.

LORENZO RUBIO was born in El Ballestero, Albacete, Spain, in 1971. He received the M.S. and Ph.D. degrees in telecommunications engineering from the Universitat Politécnica de València, Spain, in 1996 and 2004, respectively. In 1996, he joined the Communications Department, Universitat Politècnica de València, where he is currently an Associate Professor of wireless communications. His main research interest are is related to wireless communications. Specific current research topics include radiowave propagation, measurement and mobile time-varying channels modeling in vehicular applications, ultra-wideband (UWB) communication systems, multiple-input-multiple-output (MIMO) systems, and equalization techniques in digital wireless systems. He received the Ericsson Mobile Communications Prize from the Spanish Telecommunications Engineer Association for his study on urban statistical radiochannels characterization applied to wireless communications.

JUAN REIG received the Ph.D. degree from the Universitat Politècnica de València (UPV), Spain, in 2000. He has been a Faculty Member with the Department of Communications, UPV, since 1994, where he is currently a Full Professor of telecommunication engineering. He is also a member of the Electromagnetic Radiation Group (GRE), Institute of Telecommunications and Multimedia Applications (iTEAM). His areas of interest include fading theory, diversity, ultra-wideband (UWB) systems, vehicular communications, and millimeter-wave (mmWave) propagation.

RAUSLEY ADRIANO AMARAL DE SOUZA was born in Brazil, in 1972. He received the B.S.E.E. and M.Sc. degrees from the National Institute of Telecommunications (INATEL), Brazil, in 1994 and 2002, respectively, and the Ph.D. degree from the School of Electrical and Computer Engineering, State University of Campinas (UNICAMP), Campinas, Brazil. From 1995 to 2001, he was a Purchase Manager with Leucotron Equipamentos Ltda. He joined INATEL, in 2002, where he is currently a Full Professor. He is also a Productivity Research Fellow of the National Council for Scientific and Technological Development (CNPq), Brazil. Since 2015, he has been with the Radiocommunication Reference Center, whose researches are concentrated on the fifth-generation (5G) systems. He has coauthored the book entitled *Digital Transmission - Principles and Applications* (Portuguese: Erica, 2014). His general research interests include wireless communications, fading channel modeling and simulation, diversity systems, and spectrum sensing in cognitive radio systems. He is a member of the Brazilian Telecommunications Society (SBrT) and the IEEE.

MICHEL DAOUD YACOUB was born in Brazil, in 1955. He received the B.S.E.E. and M.Sc. degrees from the School of Electrical and Computer Engineering, University of Campinas (UNICAMP), Campinas, Brazil, in 1978 and 1983, respectively, and the Ph.D. degree from the University of Essex, Colchester, U.K., in 1988. He was a Research Specialist with the Research and Development Center, Telebrás, Rio de Janeiro, Brazil, from 1978 to 1985, where he was involved in the development of the Trópico digital exchange family. He joined the School of Electrical and Computer Engineering, UNICAMP, in 1989, where he is currently a Full Professor. He consults for several operating companies and industries in the wireless communications area. He has authored the books entitled *Foundations of Mobile Radio Engineering* (CRC, 1993) and *Wireless Technology: Protocols, Standards, and Techniques* (CRC, 2001) and has coauthored the book entitled *Telecommunications: Principles and Trends* (Portuguese: Erica, 1997). He holds two patents. His current research interest includes wireless communications.